

RESEARCH ARTICLE SUMMARY

PROTEIN ENGINEERING

Topological control of cytokine receptor signaling induces differential effects in hematopoiesis

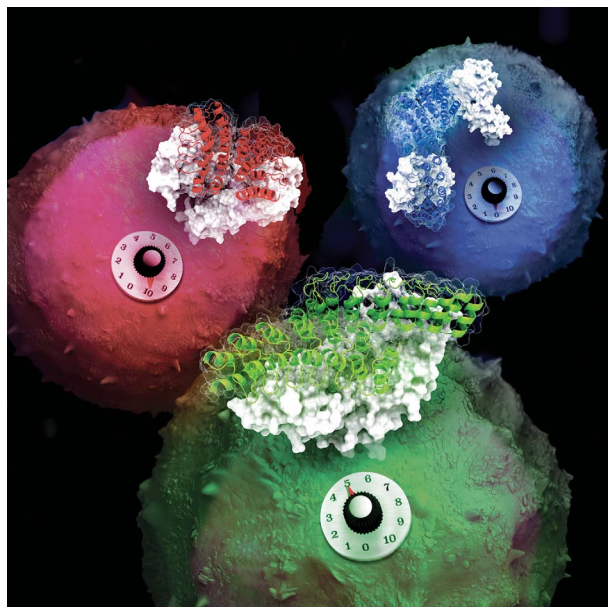
Kritika Mohan*, George Ueda*, Ah Ram Kim†, Kevin M. Jude†, Jorge A. Fallas†, Yu Guo†, Maximillian Hafer, Yi Miao, Robert A. Saxton, Jacob Piehler, Vijay G. Sankaran, David Baker‡, K. Christopher Garcia‡

INTRODUCTION: Receptor dimerization is a fundamental mechanism by which most cytokines and growth factors activate Type-I transmembrane receptors. Although previous studies have shown that ligand-induced topological changes in the extracellular domains (ECDs) of dimeric receptors can affect signaling output, the physiological relevance is not well understood. This is a difficult problem to study because an engineered ligand system does not exist that would enable a systematic exploration of the relationship between ligand-receptor dimer geometry and signaling. This question, as well as the capability of exploiting these structure-activity relationships for drug discovery, are important because most cytokines exert pleiotropic effects that limit their therapeutic utility. New approaches are needed to modulate cytokine signaling and identify clinically efficacious variants. By contrast, small-molecule ligands for G protein-coupled receptors have been successfully discovered through medicinal chemistry and used to induce conformational changes that lead to physiologically relevant biased signaling outputs. A comparable approach for dimeric receptors could open a path to new pharmacological parameters for cytokines and growth factors.

RATIONALE: In order to better understand how the extracellular structure of cytokine-receptor complexes affects downstream signaling events, we developed an engineered ligand system to precisely control the orientation and proximity of dimeric receptor complexes that would enable the measurement of structure-activity relationships between receptor dimer geometry, signaling, and function. We applied this approach to design geometrically controlled ligands to the erythropoietin receptor (EpoR)

system, a well-characterized dimeric cytokine receptor system.

RESULTS: We used the DARPin (designed ankyrin repeat protein) scaffold because of



Three different EpoR/DARPin complex topologies are shown that elicit full, partial, and null agonism. Full agonism, red; partial, green; and null, blue. The EpoR/DARPin structure shown on the green cell is from a crystal structure, whereas the complexes shown on the red and blue cells are models.

its modular nature. We isolated a high-affinity DARPin to EpoR using yeast display and in vitro evolution and determined the crystal structure of the DARPin/EpoR complex. We then converted these monomeric DARPin binding modules into C2 symmetric homodimeric agonists by incorporating in silico designed dimerization interfaces. This rigidly connected dimeric DARPin scaffold then enabled us to design a series of extended ligands through sequential insertion of ankyrin repeat “spacers” to systematically

control the relative orientation of the ECDs in the dimeric complex. The “angle” series varied the scissor angle between the two ECDs, whereas the “distance” series varied their relative proximity. The designed DARPin ligands were validated by means of x-ray crystallography for representative complexes. The systematic variation of angular and distance parameters generated a range of full, biased, and partial agonism of EpoR signaling in the human erythroid cell line UT7/EPO, as shown with flow-cytometry and immunoblotting for phosphorylated downstream effectors. In general, increasing the angle or distance between the receptor ECDs resulted in a progressive partial agonism, as measured with changes in maximum response achieved (E_{max}) and median effective concentration (EC_{50}). Biased signal transducer and activator of transcription (STAT) activation was elicited by some of the surrogate DARPin ligands. We also evaluated the effects of these DARPin agonists on differentiation and proliferation of hematopoietic stem and progenitor cells (HSPCs) that were maturing into the erythroid lineage. The partial agonists displayed stage-selective effects on HSPCs, whereas the biased agonists more selectively promoted signaling at either the early or late stages of differentiation.

CONCLUSION: We have designed a series of surrogate ligands to systematically alter receptor dimer topology and modulate signaling outputs. An important feature of these ligands is that the dimerized modules are rigidly connected, thus allowing us to determine structures of the ligand-receptor complexes, or model them accurately, and correlate precise geometries with signaling output. Some variants induce stage-selective differential signaling in primary cells. This “topological tuning” may be attributed to altered intracellular orientations of Janus kinase 2 (JAK2) relative to its substrates or mechanical distortion that leads to changes in complex stability and receptor internalization. Although our experiments do not reveal a predictive framework to relate topology to signaling, this approach can be used to empirically identify specific dimer topologies that correlate with therapeutically desirable signaling outputs for any dimeric receptor system. ■

The list of author affiliations is available in the full article online.
 *These authors contributed equally to this work.
 †These authors contributed equally to this work.
 ‡Corresponding author. Email: dabaker@uw.edu (D.B.); kcgarcia@stanford.edu (K.C.G.)
 Cite this article as K. Mohan et al., *Science* 364, eaav7532 (2019). DOI: 10.1126/science.aav7532

RESEARCH ARTICLE

PROTEIN ENGINEERING

Topological control of cytokine receptor signaling induces differential effects in hematopoiesis

Kritika Mohan^{1*}, George Ueda^{2,3*}, Ah Ram Kim^{4,5,6,†}, Kevin M. Jude^{7,†}, Jorge A. Fallas^{2,3,†}, Yu Guo^{8,†}, Maximilian Hafer⁹, Yi Miao¹, Robert A. Saxton^{1,7}, Jacob Piehler^{9,10}, Vijay G. Sankaran^{3,5,6}, David Baker^{2,3,11,†}, K. Christopher Garcia^{1,7,12,†}

Although tunable signaling by G protein-coupled receptors can be exploited through medicinal chemistry, a comparable pharmacological approach has been lacking for the modulation of signaling through dimeric receptors, such as those for cytokines. We present a strategy to modulate cytokine receptor signaling output by use of a series of designed C2-symmetric cytokine mimetics, based on the designed ankyrin repeat protein (DARPin) scaffold, that can systematically control erythropoietin receptor (EpoR) dimerization orientation and distance between monomers. We sampled a range of EpoR geometries by varying intermonomer angle and distance, corroborated by several ligand-EpoR complex crystal structures. Across the range, we observed full, partial, and biased agonism as well as stage-selective effects on hematopoiesis. This surrogate ligand strategy opens access to pharmacological modulation of therapeutically important cytokine and growth factor receptor systems.

Cytokines are secreted proteins that mediate a wide range of functions, principally in the immune system, but they also exert many other homeostatic functions that affect mammalian physiology (1–3). As one example, hematopoiesis, the process by which blood cells are formed, is influenced at both early and late stages by a milieu of different cytokines that engage and activate specific cell-surface receptors expressed on different lineages of cells (4). When cytokines bind to their receptors, receptor dimerization triggers transphosphorylation of Janus (JAK)/TYK kinases, and subsequent

propagation of a phosphorylation cascade leading to signal transducer and activator of transcription (STAT) activation and induction of gene expression programs (3, 5). Structural and functional studies of cytokine-receptor complexes together with similar studies on growth factor dimeric receptor systems, including receptor tyrosine and serine-threonine kinases, show that a wide range of receptor dimer geometries are compatible with signaling (3, 5–9).

Given their powerful actions, many natural cytokines have been investigated as therapeutic agents. Whereas select cytokines are clinically safe and effective, such as erythropoietin (EPO) (10), most natural cytokines, especially immune cytokines, have pleiotropic effects on many different cells and stimulate multiple downstream signaling responses, resulting in toxicity or lack of efficacy (11, 12). Nevertheless, cytokines have potential as therapeutics if their actions can be harnessed, as exemplified by recent advances for cytokines such as interleukin-2 (IL-2) and IL-10 (13, 14). Recent studies, using natural and engineered ligands to both cytokine and receptor tyrosine kinase (RTK) class receptors, show that signal strength can be modulated downstream of dimeric receptors (15–18). Furthermore, select natural and synthetic mutants of cytokines such as IL-2, human growth hormone (hGH), stem cell factor (SCF), and EPO that exhibit partial and biased signaling properties have been identified (17, 19, 20). In G protein-coupled receptors (GPCRs), biased signaling is physiologically relevant and generally depends on binding of small-molecule ligands, making this exploitable as a drug discovery strategy by using medicinal

chemistry (21). Finding small-molecule drugs is not currently feasible for Type-I transmembrane receptors that bind to protein ligands, such as cytokines, through large extracellular domains (ECDs). Nevertheless, ligand engineering strategies that take advantage of the potential for biased signaling behavior by dimeric cytokine receptors could be used as probes to better understand cytokine receptor signaling biology but also may have therapeutic potential.

The overall geometry of the cytokine receptor dimer can influence the strength of the downstream signal (6, 22–24); however, approaches do not exist to precisely control the orientation and proximity of ligand-receptor complexes. The ability to topologically control receptor dimerization could open access to a new pharmacologic metric for assessing structure-activity relationships of cytokine and growth factor receptor signaling. Previous studies have shown that intact antibodies (25, 26) and diabodies can act as surrogate cytokine agonists capable of modulating signaling outputs through receptor dimerization (24, 27), but their segmental flexibility prevents control of the precise geometry or distance between monomers.

We integrated a previous protein-binding scaffold technology, termed DARPin (designed ankyrin repeat protein) (28), with protein design and engineering approaches to create a self-assembling, rigidly connected dimeric scaffold that enables precise control of the relative orientations of the receptor ECDs in a dimeric complex (Fig. 1A). We focused on the erythropoietin receptor (EpoR), which plays a critical role in erythroid lineage commitment and differentiation to produce mature red blood cells (RBCs) (20). We found that systematic variation of angular and distance parameters of the DARPin-based agonists leads to partial and biased agonism of the EpoR signal. Furthermore, this variation in geometry has allowed us to selectively activate EpoR signaling at specific stages of hematopoiesis. Collectively, these studies offer a general strategy for the regulation of cytokine receptor signaling through topological control of the receptor dimer that can be applied to other dimeric receptor systems.

Results

Selection of monomeric DARPins selective for EpoR

Our overall strategy was to engineer a protein module that binds with high affinity to a cytokine receptor ECD and subsequently design the module to form a range of dimeric geometries that would in turn constrain the dimerization geometry of the bound receptor (Fig. 1A). We focused on a well-characterized system, human EpoR, as our cytokine receptor target for topological tuning. We chose DARPins as the binding scaffold because they are modular, which enables size variation (28), and have been used to design self-assembling oligomers (29). A DARPin molecule typically consists of “X” number of ankyrin repeats flanked by N- and C-terminal capping regions, resulting in “NXC” DARPins. Each ankyrin repeat is formed by 33 amino

¹Department of Molecular and Cellular Physiology, Stanford University School of Medicine, Stanford, CA 94305, USA.

²Department of Biochemistry, University of Washington, Seattle, WA 98195, USA. ³Institute for Protein Design, University of Washington, Seattle, WA 98195, USA. ⁴Division of Hematology/Oncology, The Manton Center for Orphan Disease Research, Boston Children's Hospital, Harvard Medical School, Boston, MA 02115, USA. ⁵Department of Pediatric Oncology, Dana-Farber Cancer Institute, Harvard Medical School, Boston, MA 02115, USA. ⁶Broad Institute of MIT and Harvard, Cambridge, MA 02142, USA. ⁷Howard Hughes Medical Institute, Stanford University School of Medicine, Stanford, CA 94305, USA. ⁸State Key Laboratory of Medicinal Chemical Biology and College of Pharmacy, Nankai University, Tianjin, People's Republic of China.

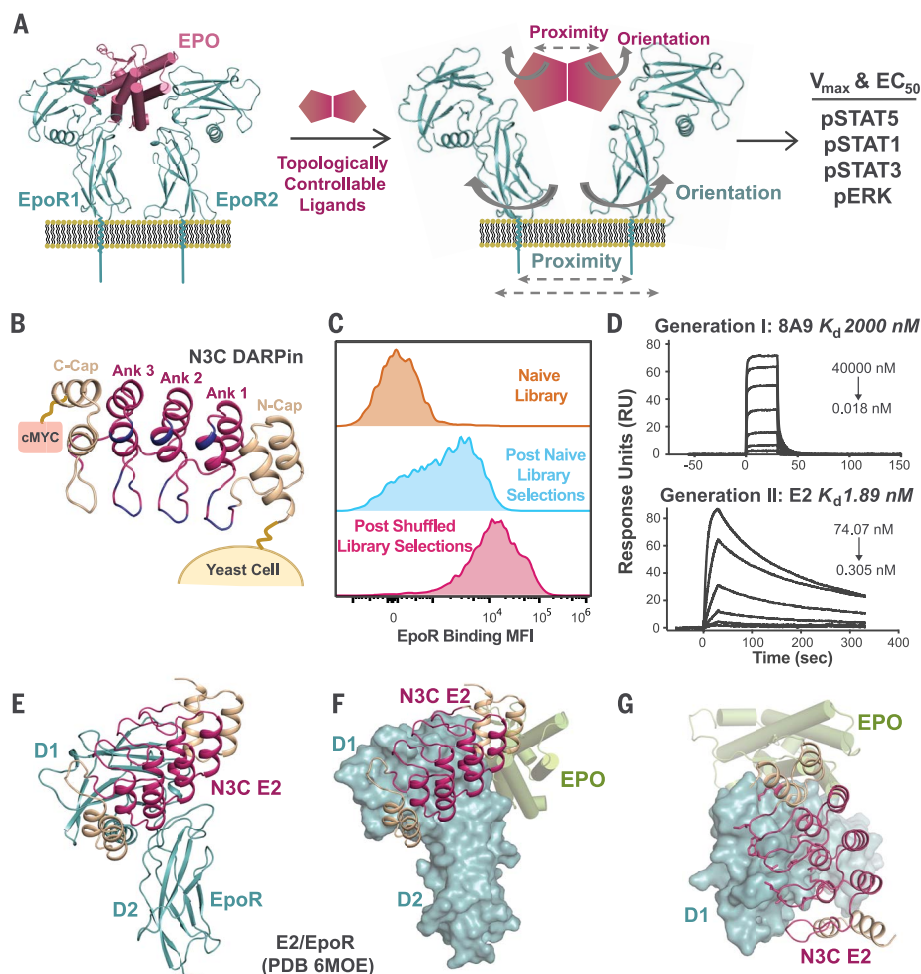
⁹Division of Biophysics, Department of Biology, University of Osnabrück, 49076 Osnabrück, Germany. ¹⁰Center for Cellular Nanoanalytics, University of Osnabrück, 49076 Osnabrück, Germany. ¹¹Howard Hughes Medical Institute, University of Washington, Seattle, WA 98195, USA. ¹²Department of Structural Biology, Stanford University School of Medicine, Stanford, CA 94305, USA.

*These authors contributed equally to this work. †These authors contributed equally to this work.

‡Corresponding author. Email: dabaker@uw.edu (D.B.); kcgarcia@stanford.edu (K.C.G.)

Fig. 1. Engineering and characterization of high-affinity DARPin binding to EpoR.

(A) An overview of our topological control strategy, using EpoR as a model system to investigate modulation of signaling responses. **(B)** Schematic representation of the yeast-displayed N3C DARPin construct used for library generation. The randomized positions are shown in blue. **(C)** Histograms of yeast-displayed naive N3C library, pool of DARPin clones after in vitro evolution, and pool of shuffled library clones after in vitro evolution binding to EpoR. MFI, mean fluorescence intensity. **(D)** Representative surface plasmon resonance sensograms for pre- and post-shuffled library N3C DARPin clones binding to EpoR. K_d , dissociation constant. **(E)** Structure of N3C E2 binding to EpoR. **(F)** The structure of E2/EpoR (PDB 6MOE) is aligned with EPO/EpoR to indicate relative binding sites of the two ligands. EPO is depicted as green cylinders. **(G)** The intimate shape complementarity of E2 binding to EpoR is depicted with the side chains shown for key interacting E2 residues.



acids and consists of a β turn followed by two antiparallel α helices. Twenty-seven of these positions are highly conserved in naturally occurring ankyrin repeats and crucial to maintaining the repeat protein framework (30, 31), whereas the remaining six positions can support randomization for library generation (Fig. 1B, blue residues). We developed two yeast-displayed DARPin libraries, N2C and N3C (Fig. 1B and fig. S1), which were screened against EpoR ECD, resulting in a set of low-affinity ligands with dissociation constants (K_d) in the micromolar range (Fig. 1C and fig. S2). A combination of random mutagenesis by means of error-prone polymerase chain reaction (PCR) and DNA-shuffling techniques resulted in a $>10^4$ -fold increase in affinity of individual clones (Fig. 1, C and D). The highest-affinity clone, N3C-E2, was expressed in *Escherichia coli*, and its affinity was measured with surface plasmon resonance (SPR). E2 binds to EpoR ECD with a 1.89 nM K_d , providing a >1000 -fold increase in binding affinity relative to 8A9 (Fig. 1D). We denote this DARPin as NEEEC, comprising three EpoR binding ankyrin repeats, EEE, and the N- and C-terminal capping regions.

The crystal structure of NEEEC (Fig. 1, E to G, and table S1) shows that it binds to the EpoR membrane-distal D1 domain with a 1:1 stoichi-

ometry, at a site different but overlapping with the EPO binding site, using three ankyrin repeat domains. The β turn loop regions of the ankyrin domains engage the top of the D1 domain, whereas the helical regions pack against the side of the D1 domain with high shape complementarity and extensive buried surface area.

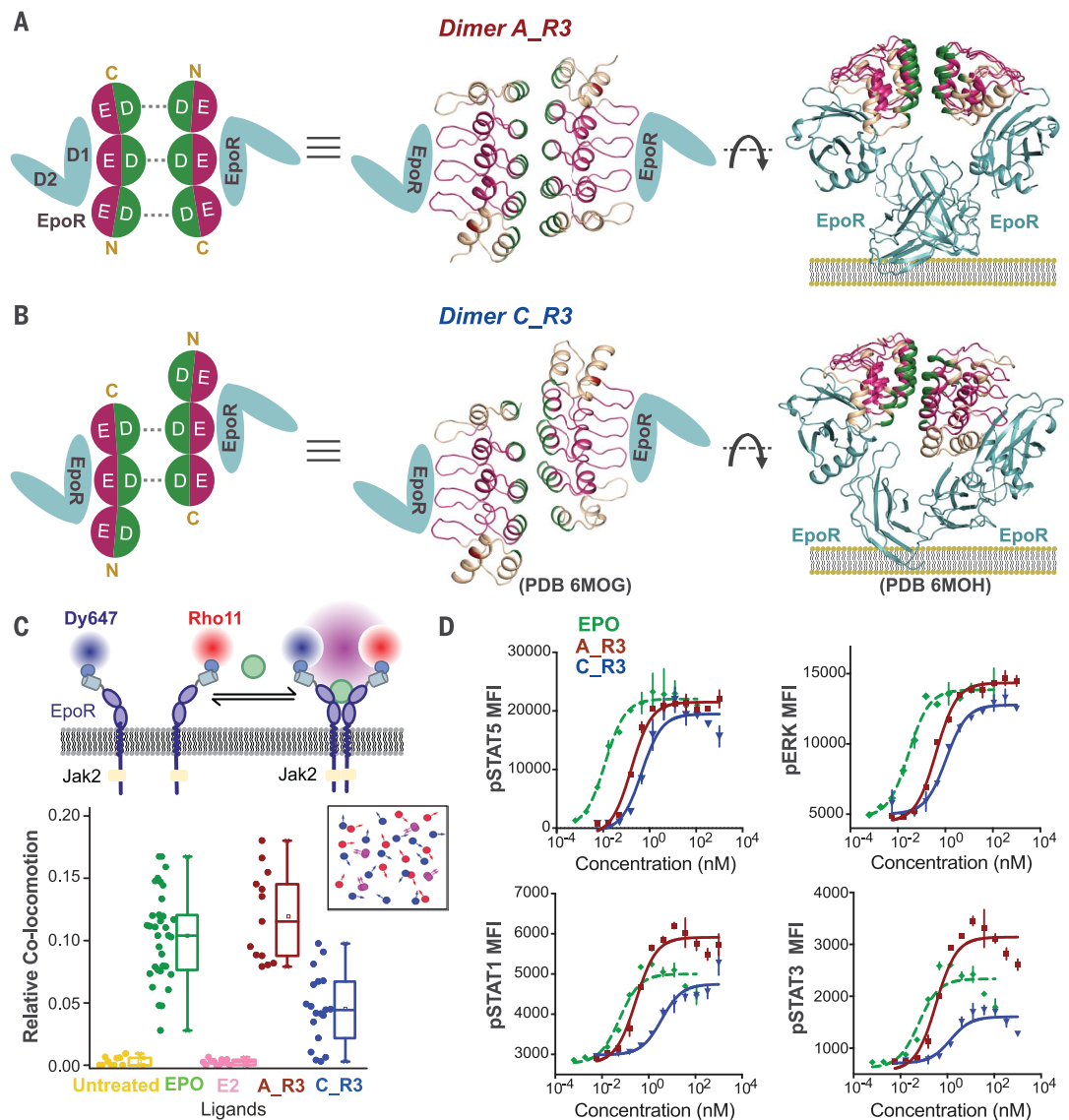
Generation of agonist DARPin dimers

In order to endow the monomeric DARPin NEEEC with the ability to dimerize EpoR and act as an agonist, it was converted into two different homodimeric geometries by incorporating designed dimer interfaces at the nonbinding face of the DARPin (29). The interface mutations provide hydrophobic side chain interactions at nonsolvent accessible positions and salt bridge interactions at solvent-exposed positions, which results in the formation of noncovalent self-assembling homodimers, A_R3 and C_R3, where Rx indicates the number of ankyrin repeats (Fig. 2, A and B, and figs. S3 and S4). The A and C dimers differ by a shift in the relative orientation of the monomers across the C2 axis. Dimer C_R3 has an offset of one repeat at the dimerizing interface compared with dimer A_R3, providing a twist of 30° in the relative orientation of the two di-

merized EpoR ECDs (Fig. 2B and fig. S5). The formation of the C_R3 DARPin dimer and a 2:2 C_R3/EpoR complex was confirmed with size exclusion chromatography, and crystal structures were determined to 1.2 and 3.2 Å resolution, respectively. We assessed the ability of the DARPin dimers to dimerize EpoR on the surface of live cells using single-molecule total internal fluorescence (TIRF) microscopy (Fig. 2C and fig. S6). For this purpose, EpoR fused to an N-terminal monomeric XFP (mXFP)-tag was expressed in HeLa cells at physiologically relevant densities (~ 0.5 to 1 copies/ μm^2 ; ~ 1000 to 2000 copies/cell) and labeled by means of specific nanobodies. EpoR dimerization was quantified through dual-color cotracking of individual receptor dimers (fig. S6 and movie S1). Like EPO, both ligands showed ligand-dependent dimerization of EpoR at the cell surface, although C_R3 was less efficient than A_R3 (Fig. 2C, fig. S6, and movie S2).

Dimerization of EpoR initiates a sequential cascade of phosphorylation events, the initial membrane proximal step being phosphorylation of JAK2, followed by tyrosines on the EpoR intracellular domain (ICD), and then principally activation of STAT5 and extracellular signal-regulated kinase (ERK), and to a lesser extent STAT1 and STAT3. Other pathways not surveyed here,

Fig. 2. Dimerization scaffolds for E2 resulting in agonism. (A and B) Point mutations (shown in green) inserted on the rear face of the DARPin lead to the formation of noncovalent homodimers with two different geometries. A schematic representation is shown for formation of the 2:2 DARPin:EpoR complex. An N3C DARPin containing three ankyrin repeats is represented by three spheres. The EpoR binding face of the ankyrin repeat is shown as “E” (pink), and the dimerizing face is shown as “D” (green), whereas the two EpoR domains D1 and D2 are shown in teal. The dimer interface for C_R3 (PDB 6MOG) is offset by one repeat providing additional twist in the EpoR geometry in C_R3/EpoR (PDB 6MOH) (B). (C) Ligand-induced dimerization of EpoR on the surface of cells, as observed with dual-color single-molecule TIRF microscopy. (Inset) The method of single-molecule cotracking analyses. (D) Dose-response curves for STAT1/3/5 and ERK activation performed in UT7/EPO cells stimulated with EPO, A_R3, or C_R3 for 15 min. Data are mean \pm SD for two independent replicates. A sigmoidal dose-response analysis was preferred over Gaussian distribution because only some ligands demonstrate a decrease in MFI values at high concentrations.



including mitogen-activated protein kinase (MAPK) and phosphatidylinositol 3-kinase (PI3K), are also activated by EPO. We analyzed the phosphorylation levels of various downstream effectors on the human erythroid cell line, UT7/EPO (32), using phospho-flow cytometry (Fig. 2D). Monomeric DARPins do not dimerize EpoR, generating no pSTAT5 signal. Both DARPin dimers induce comparable efficacy (E_{\max} ; the maximum response achieved) compared with EPO for pSTAT5 and pERK. Dimer A_R3 exhibits a higher E_{\max} for pSTAT1 and pSTAT3 than EPO, whereas dimer C_R3 exhibits a lower E_{\max} (Fig. 2D). Thus, the relatively small orientational differences between dimers A_R3 and C_R3 result in apparent signaling differences.

Topological control of EpoR dimerization geometry

To move toward topological control, we designed a series of NEEEC homodimers, systematically

varying the scissor angle (rotation) and proximity between EpoR ECD monomers (distance). We designed three different DARPin dimer extension series to interrogate signaling as a function of these parameters in a systematic manner (Fig. 3). The “angle” series is intended to pivot the EpoR dimer in a scissorlike manner (Fig. 3, top). The “distance” series is intended to separate the EpoR subunits in the dimer while not substantially changing the dimer angle (Fig. 3, middle). The “mono-extended” series differs from the angle and distance series in that both EpoR subunits are bound to one extended DARPin (monomeric) that contains two EpoR binding sites (Fig. 3, bottom).

Systematic variation in each of these parameters can be achieved by inserting nonbinding “P” repeats derived from the consensus ankyrin repeat sequence, which changes the relative positions of the EpoR binding repeats across the designed dimerization interface in predictable ways that can be modeled. Because of the nonplanar, helical

nature of the DARPin molecule (33), this results in dimers in which the two EpoR binding interfaces assume different separations and orientations (Fig. 3). To engineer the “angle” series, one or more P repeats are inserted at the C-terminal end to provide DARPins such as NEEEP_C, (Fig. 3, top, and fig. S7). The dimerizing residues (indicated with underline) are engineered on the same terminus as that of the P repeat insertions. As the added repeats grow along a helical path, this results in the generation of a series of dimers with variation in the angle between the two receptor ECD monomers. The resultant extended dimer is termed A_angle_Rx, where A indicates the designed dimer interface, and “x” indicates the total number of ankyrin repeats. For example, NEEEP_C is termed A_angle_R5.

To engineer the “distance” series, the nonbinding P repeats are inserted at the N terminus—for example, NPP...EEEC (Fig. 3, middle, and figs. S8 and S9). The dimerizing residues are also

placed at the N terminus so that this results in two helical DARPins growing in opposite directions with a twofold symmetry. With the addition of more P repeats, the binding repeats move further apart, leading to a distance-based series, termed *A_dist_Rx*.

Last, we designed a monomeric, extended DARPIn with two binding sites included on the same DARPIn chain (Fig. 3, bottom, and fig. S9),

but with the bound EpoRs in an inverted rotational orientation relative to the dimerized DARPins (“face-to-back” versus “face-to-face”). The two sets of EpoR binding repeats are positioned at the two termini, separated by a series of P repeat insertions that can be varied in number to control the distance between the two receptors—for example, NEEEEPPP...EEEC. These monomeric extended DARPins are termed *M_Rx*,

where “x” indicates the total number of ankyrin repeats.

Each of the dimers was expressed in *E. coli*, purified through size-exclusion chromatography, and bound to EpoR with similar affinities, as measured with SPR (figs. S7 to S9). To validate the designs and also to determine whether any clashes were apparent between the EpoR receptors, we determined six crystal structures of

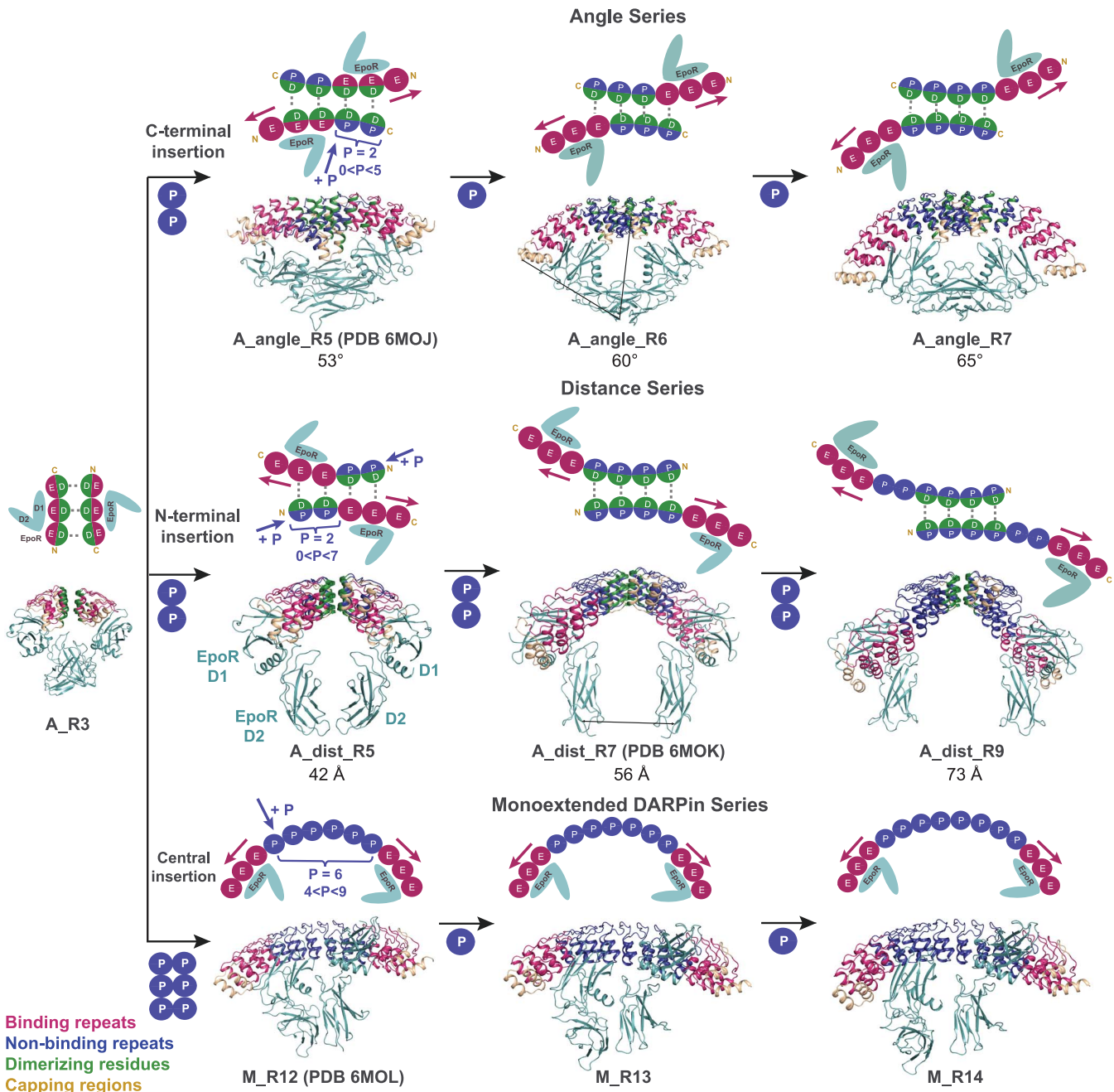


Fig. 3. Topological control of EpoR geometry. Three different series were designed to systematically modify the different components of receptor dimerization—specifically, angle (*A_angle_Rx*), distance (*A_dist_Rx*), and inversion of geometry (*M_Rx*). The insertion (indicated by blue arrows) of nonbinding “P” ankyrin repeats (blue) at different termini of nonplanar DARPins leads to different receptor dimer topologies. The relative movement

of the two receptors with the insertion of P repeats is indicated by pink arrows. The series are generated through stepwise insertion of one P repeat, and the nomenclature “Rx” indicates the total number of ankyrin repeats. The cartoon representations are shown along with the crystal structures for one representative member per series: *A_angle_R5* (PDB 6MOJ), *A_dist_R7* (PDB 6MOK), and *M_R12* (PDB 6MOL).

representative members of the series: the apo C_R3 dimer (1.2 Å resolution) as well as EpoR complexes with C_R3 (3.46 by 3.16 Å resolution), A_angle_R5 (3.39 by 2.45 Å resolution), C_angle_R5 (3.0 by 2.0 Å resolution), A_dist_R7 (5.1 Å resolution), and M_R12 (4.58 by 3.14 Å resolution) (Fig. 3, fig. S10, and tables S1 and S2). The structures validate the DARPIn dimer designs, albeit with minor rigid body variations because of lever arm effects centered at the DARPIn dimer interface (fig. S11), allowing us to model the full geometry series based on the known effects of P repeat insertion. In all of the structures determined, whereas the D1 domain of EpoR maintains a rigid contact with the DARPIn, the D2 domain exhibits some segmental flexibility and adapts variable positions relative to D1 that are likely influenced by crystal packing. We measured a range of 28° variation in D2 position (fig. S12), which is consistent with that observed in previously published structures of EpoR.

EpoR angle series

The basic building block of the angle series is A_R3 with zero P repeats (NEEEEC), and subsequent members with one or more P repeats added in, A_angle_R4 (NEEEPC) through A_angle_R7 (NEEEPPPC), progressively tilt each EpoR monomer toward the membrane (Fig. 4A). As measured with phospho-flow cytometry in UT7/EPO cells, the dimer A_angle series exhibits a progressive reduction in E_{\max} levels of STAT5 phosphorylation as the EpoR dimer scissor half-angle increases from ~38° (A_R3) to 72° (A_angle_R9) (Fig. 4, A and B). Dimers A_angle_R4 and A_angle_R5 act as partial agonists, whereas A_angle_R7 does not elicit a signal detectable with flow cytometry. Similarly, the C_angle series shows by means of flow cytometry a stepwise decline in activation that is confirmed with immunoblotting (fig. S13). In addition to the reduction in E_{\max} , the effects of increase in angle are also reflected by changes in median effective concentration (EC_{50}), which is defined as the ligand concentration that provides 50% of maximal response (E_{\max}). A progressive right shift was observed for the EC_{50} values, implying the need for a higher ligand concentration to generate the same levels of signal, despite all of the dimers having the same affinity for EpoR, as measured with SPR by using soluble EpoR ECD (fig. S7). We speculate that as the scissor angle between EpoRs becomes more extreme, strain is induced as a result of cell membrane constraints, and this is reflected in less efficient bivalent complex formation.

We also analyzed a broad panel of downstream phosphorylated proteins using phosphorylation barcoding, which provides a broad “footprint” of relative signal strengths. This data showed a similar trend of reduced E_{\max} with increasing scissor angle (Fig. 4C, fig. S13B, and tables S3 and S4). At higher concentrations, a bias was observed for STAT1 and STAT3 by A_R3 compared with EPO by means of phospho-flow. Because the phosphorylation barcoding data are

intended to convey qualitative relative signal strengths, we more precisely confirmed with immunoblotting the appearance of signal bias (Fig. 4D). A similar STAT1 bias was observed for A_angle_R5 and C_angle_R4, with extremely high pSTAT1 signal at highest concentrations (fig. S13). Immunoblot analysis of cell lysates further verified the STAT1 bias observed for A_R3, A_angle_R5, and C_angle_R4 compared with EPO (Fig. 4D and figs. S13C and S14).

EpoR distance series

The basic building block of the distance series is A_R3 with zero P repeats (NEEEEC), and subsequent members incorporate one or more P repeats: A_dist_R4 (NPEEEEC) through A_dist_R9 (NPPPPPEEEEC) (Fig. 5A). Contrary to the angle series in which a reduction in pSTAT5 and pERK E_{\max} was observed, the first few members of A_dist exhibit the same E_{\max} despite the increased distance between the receptors (Fig. 5B). Instead, the effects of the distance are reflected in a right shift in the EC_{50} values. Furthermore, a bias toward higher pSTAT1 and pSTAT3 E_{\max} than EPO or other distances was observed for A_dist_R5 (figs. S14 to S16). Analysis of a panel of downstream phosphorylated proteins by means of phospho-barcoding reflected the above trends, in which the strong bias was observed for STAT1 for the A_dist_R5 ligand (Fig. 5, C to E; figs. S14 and S15; and table S5). The biased and prolonged pSTAT1 response for A_dist_R5 was further verified through immunoblotting with 15- and 60-min ligand treatments (Fig. 5D) and may be attributable in part to the differential intracellular processing rate for the internalized receptors (Fig. S17). In general, ligands with faster internalization of cell-surface EpoR upon ligand treatment showed a more potent response. Furthermore, with an increase in angle or distance, a decrease in activity was observed, which correlates with the slower rate of internalization of the receptor. Recycling of EpoR back to the surface is slower for A_dist_R5 than other DARPIn ligands. For the distance series, the right shift of the EC_{50} was surprising because we would not imagine strain on the dimer through pure translation of the receptors to wider intermonomer distances unless there was receptor preassociation that could present an energy barrier to separation. Although we did not see EpoR predimerization with single-molecule TIRF microscopy, increasing the distance may interfere with weak synergistic interactions between the receptor subunits, possibly mediated by the transmembrane domains (34, 35).

Inverted EpoR geometry

We assessed the impact on signaling of relative EpoR ECD rotation with respect to one another while maintaining an approximately similar distance. In the native EPO/EpoR dimer structure, the receptors are face-to-face. Having validated the design of a face-to-back orientation with the crystal structure of the DARPIn M_R12/EpoR complex (Fig. 3), we assessed face-to-back orientation while maintaining a close intermonomer

distance (Fig. 5F) by comparing the signaling response for A_dist_R6 (face-to-face dimer, distance 49 Å) and M_R11 (face-to-back dimer, distance 53 Å), where M_R11 is a mono-extended DARPIn containing two EpoR binding sites separated by five ankyrin repeats, NEEPPPPPEEEEC. M_R11 delivers an extremely weak pSTAT5 signal (Fig. 5G), suggesting that the face-to-face orientation appears to be favorable for the intracellular JAK2 to transphosphorylate within an EpoR dimer, thus more effectively initiating signaling. These experiments show that rotational reorientation of the receptor ECDs can profoundly affect signaling output, which is consistent with previous studies in other systems using chimeric receptors (23) but now provides a ligand-mediated approach to exploit this parameter on natural, unmodified receptors.

Effects of designed ligands on erythropoiesis

Erythropoiesis begins with lineage commitment of hematopoietic stem and progenitor cells (HSPCs) into the erythroid lineage, and cells progressively differentiate and mature to become RBCs (Fig. 6A). This process of RBC development can be faithfully recapitulated in vitro by culturing human primary HSPCs with various cytokines over 2 to 3 weeks (Fig. 6A) (36, 37). As a main driver of RBC development, EPO plays a role in all aspects of this process, from lineage commitment to terminal maturation (Fig. 6A) (38, 39). Therefore, distinct stages of erythroid maturation may have differences in EPO signaling.

Using DARPins that either increased the distance or altered interaction angles between EpoR dimers, we found a graded reduction in overall erythroid differentiation and cellular expansion (Fig. 6B and fig. S18). Looking at overall erythroid differentiation by using flow cytometry allowed us to assess the kinetics of HSPC commitment into the erythroid lineage and the continuation of erythroid terminal maturation throughout the culture. In addition, proliferation is one of the important hallmarks in erythropoiesis that is coupled with the overall differentiation efficacy. Therefore, these analyses together in a time-dependent manner can give us further insights into stage-selective dependencies of specific EpoR activities in erythropoiesis.

This range of erythroid differentiation efficacy stimulated by various DARPIn series was assessed by using two markers: CD71, a marker of early erythroid commitment, and CD235a or glycophorin A, a marker of terminal erythroid maturation (Fig. 6C). The majority of cells cultured with EPO, A_R3, A_angle_R4, C_R3, and A_dist_R5 differentiated into CD235a⁺ erythroid cells, whereas the later members of the series (wider angle or farther distance of the EpoR dimer) impaired or failed to effectively promote erythroid commitment and differentiation (Fig. 6C). Consistent with the pattern we observed with flow cytometry for cell surface markers, treatment of cells with agonists that resulted in delayed or impaired erythroid differentiation

also resulted in reduced cellular proliferation (Fig. 6D). The cells cultured with EPO, A_R3, or A_dist_R5 showed at maximally potent concentrations very similar erythroid differentiation efficacy on differentiation day 5 (early phase of erythropoiesis), with CD235a⁺CD71⁺ of 31.7 ± 1.0%, 28.0 ± 1.6%, and 30.9 ± 0.6%, respectively (Fig. 6E). However, on differentiation day 12, cells cultured with A_dist_R5 showed lower CD235a⁺CD71⁺-positive cells compared with EPO and A_R3. Cells cultured with A_dist_R5

exhibited 1.7 ± 0.1% CD235a⁺CD71⁻ cells, whereas cells with the recombinant EPO and A_R3 showed 28.7 ± 2.0% and 26.8 ± 1.6% in this population, respectively, indicating the impairment of terminal erythropoiesis in the late stage with A_dist_R5 (Fig. 6E). Furthermore, cells cultured with A_dist_R5 demonstrated reduced proliferation, relative to EPO or A_R3, in the later stages of the erythroid differentiation culture (Fig. 6D), demonstrating that A_dist_R5 specifically promotes early erythropoiesis with impairments at

the later stages. In addition, C_R3 promoted early erythropoiesis poorly but showed increased differentiation efficacy in the later stages (fig. S18), suggesting that this ligand selectively promotes the later stages of erythropoiesis while having reduced stimulation earlier. Collectively, these results demonstrate how topological alterations in EpoR dimerization can selectively promote effective signaling at specific stages of human erythropoiesis but fail to effectively enable differentiation and proliferation at other stages.

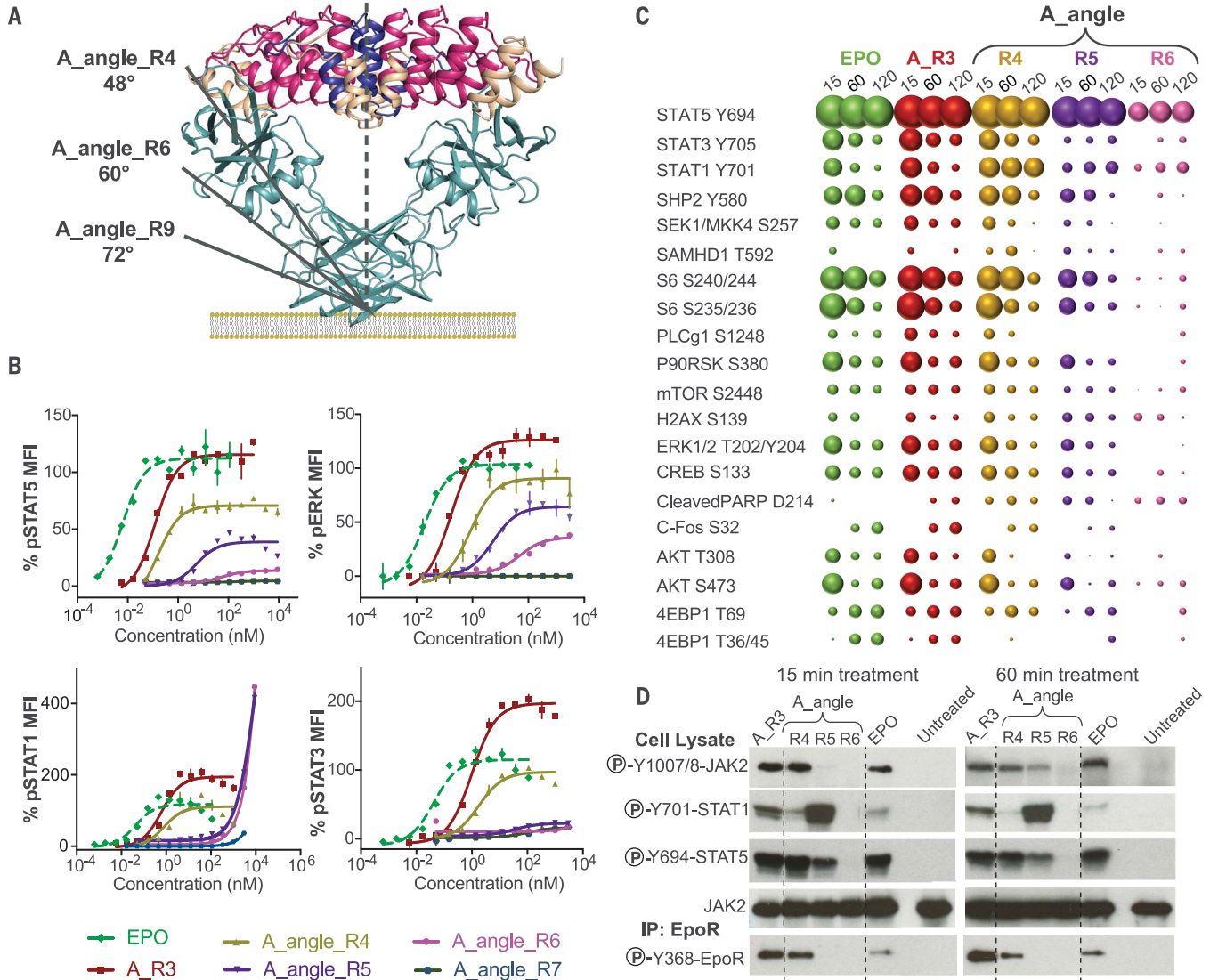


Fig. 4. Signaling responses induced through variation in EpoR dimer angle. (A) Addition of P repeats at the C terminus leads to increase in the angle between the EpoR ECDs, as shown. (B) Signaling bias observed for the dose-response curves for the angle series. Shown are percentage of pSTAT1/3/5 and pERK induced by the various DARPin ligands relative to EPO in UT7/EPO cells. Data are mean ± SD for two independent replicates. A sigmoidal dose-response analysis was preferred over Gaussian distribution because only some ligands demonstrate a decrease in MFI values at high concentrations. (C) Bubble plot representation of the various downstream pathways activated by EPO or the DARPin ligands in UT7/EPO cells with 15, 60, and 120 min of stimulation. The size of the bubble correlates to the signal strength determined as the log₂ value of the ratio of the signal generated by the ligand to unstimulated cells. (D) The levels of phosphorylated downstream effectors were analyzed in the cell lysates by immunoblotting after 15 and 60 min of ligand treatment. EpoR-immunoprecipitates were analyzed by immunoblotting for phosphorylation of specific Tyr residues in the EpoR ICD. The dashed lines indicate the sites where the immunoblots were cropped for clarity. The uncropped immunoblots are included in fig. S14.

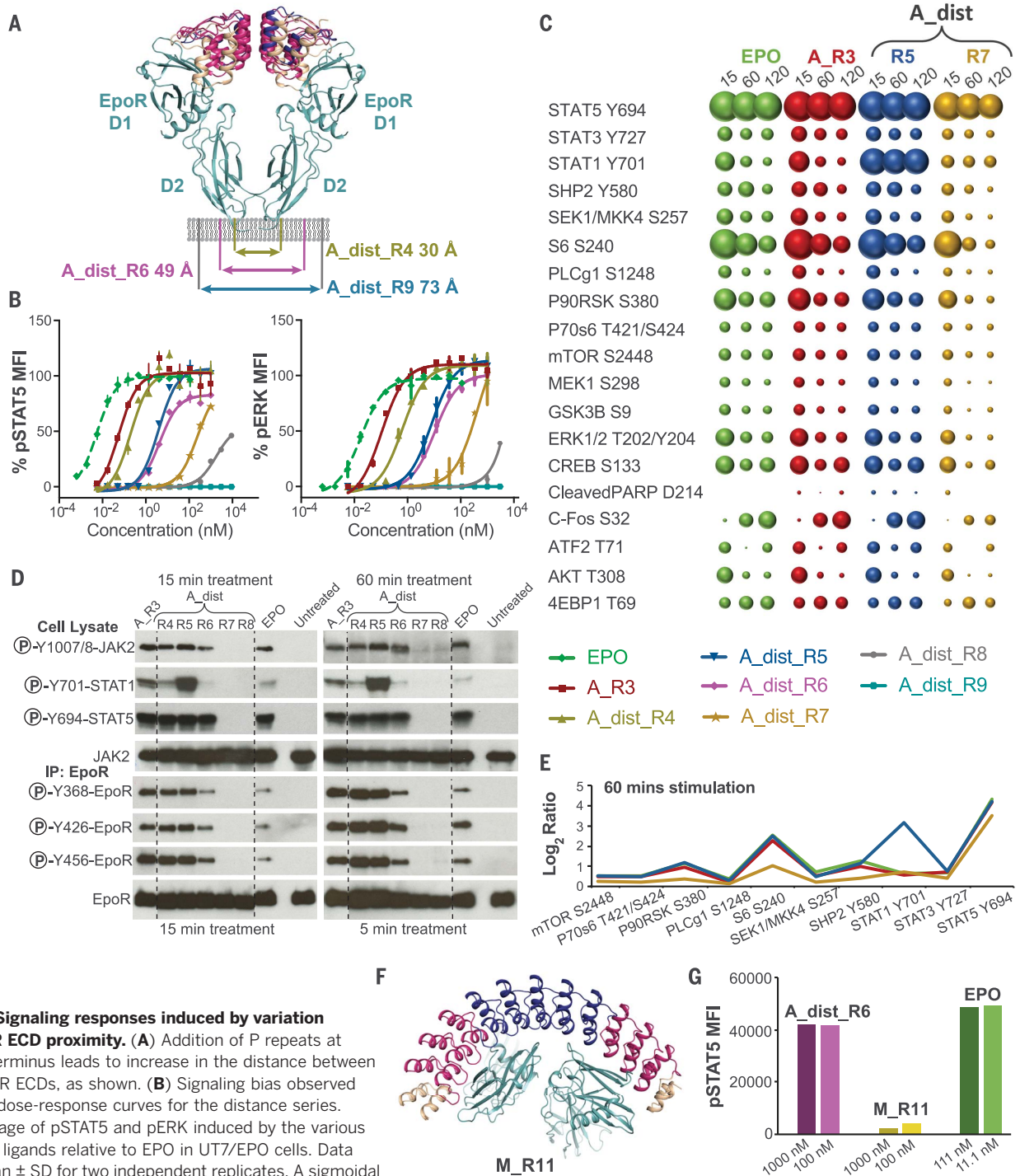


Fig. 5. Signaling responses induced by variation in EpoR ECD proximity.

(A) Addition of P repeats at the N terminus leads to increase in the distance between the EpoR ECDs, as shown. (B) Signaling bias observed for the dose-response curves for the distance series. Percentage of pSTAT5 and pERK induced by the various DARPin ligands relative to EPO in UT7/EPO cells. Data are mean \pm SD for two independent replicates. A sigmoidal dose-response analysis was preferred over Gaussian distribution because only some ligands demonstrate a decrease in MFI values at high concentrations. (C) Bubble plot representation of the various downstream pathways activated by EPO or the DARPin ligands in UT7/EPO cells with 15, 60, and 120 min of stimulation. The size of the bubble correlates to the signal strength. (D) Immunoblot analysis of phosphorylated downstream effectors in cell lysates after 15 and 60 min of ligand treatment, and analysis of EpoR-immunoprecipitates for phosphorylation of specific Tyr residues in the EpoR ICD. The dashed lines indicate the sites where the immunoblots were cropped for clarity. The uncropped immunoblots are included in fig. S14. (E) The log₂ value of the ratio of the signal generated by the ligand to unstimulated cells at 60 min. (F) The model for M_R11 binding to EpoR. (G) Inversion of the relative geometry of the EpoR ECDs for the mono-extended M_R11, which possesses a similar inter-ECD distance to A_{dist}_R6, leads to a complete loss of pSTAT5 activity.

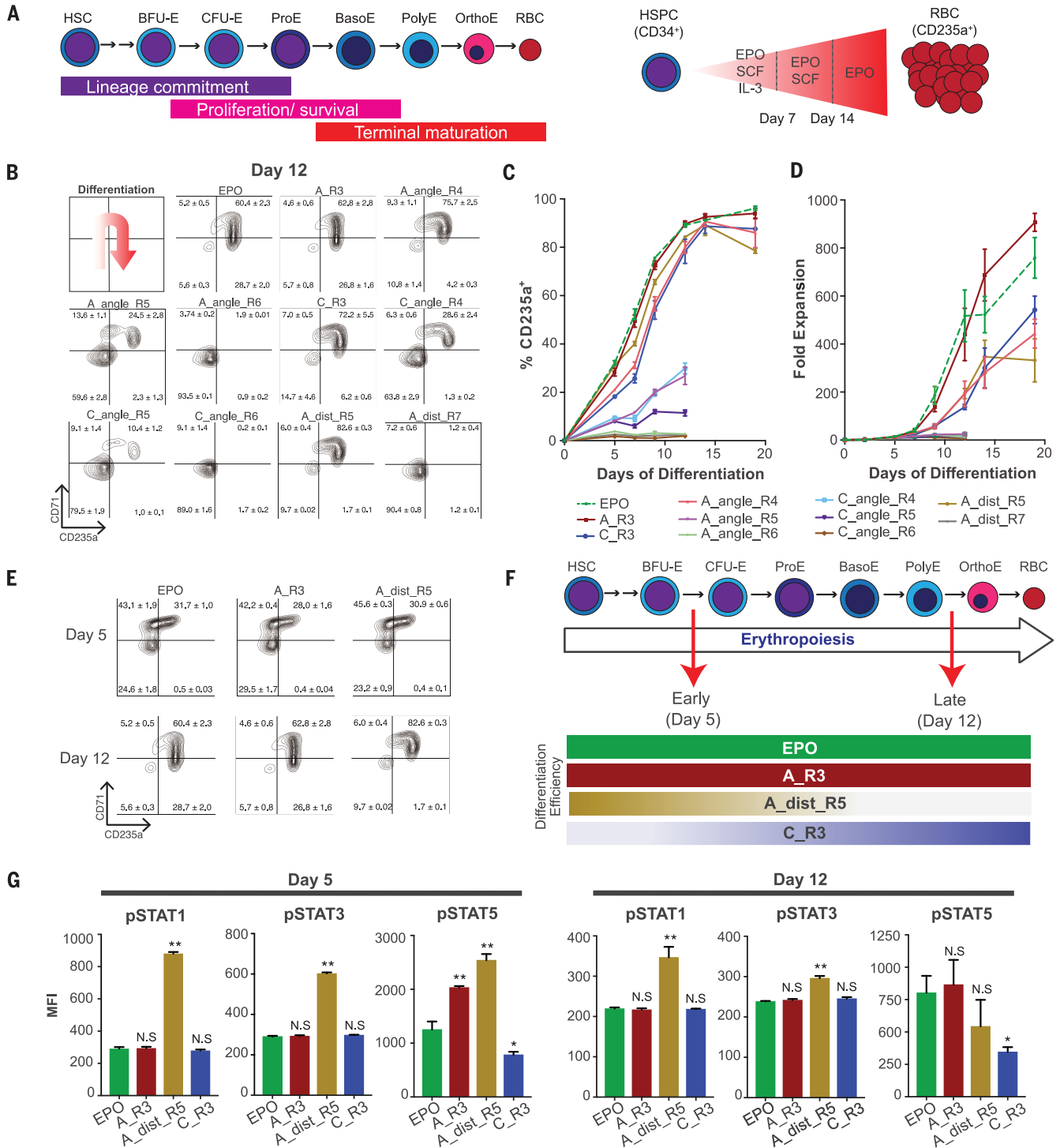


Fig. 6. Effects on hematopoiesis of topologically controllable EpoR ligands. (A) Overview of erythropoiesis and in vitro differentiation of human primary hematopoietic cells. (B) Erythroid differentiation from CD34⁺ HSPC with surrogate EPO ligands. Differentiation has been assessed with flow cytometry with the markers CD71 and CD235a at day 12 of differentiation. Means ± SEM for three independent experiments are shown. (C) Total CD235a⁺ cells and (D) overall cell proliferation during erythroid differentiation. Data are means ± SEM for three independent experiments (n = 2 independent experiments for A_dist_R5). (E) Flow

cytometry analysis of erythroid differentiation by EPO, A_R3, or A_dist_R5 at different time points are shown with flow cytometry analysis. Means ± SEM for three independent experiments are shown. (F) Experimental scheme of analyzing ligand-stimulated downstream signaling stimulated by EPO, A_R3, A_dist_R5, and C_R3 during erythropoiesis. (G) Total MFI of pSTAT1/3/5 stimulated with EPO, A_R3, A_dist_R5, or C_R3 at early (day 5 of differentiation) and late (day 12 of differentiation) erythropoiesis. Data are (mean ± SEM) for three independent experiments [(B), (E), and (G)]. **P < 0.01, *P < 0.05.

These phenotypes led us to ask whether there may be biased signaling responses downstream of EpoR that correlate with such effects (Fig. 6F). Erythroid cells stimulated with A_dist_R5 showed higher activation of STAT1/3/5 than with the recombinant EPO or A_R3 in the early stages (day 5). However, erythroid cells stimulated with A_dist_R5 showed higher activation of STAT1 and STAT3, but lowered pSTAT5 was observed in the late stage of erythropoiesis (day 12) relative to EPO or A_R3 in the late stage of erythropoiesis (Fig. 6G). Furthermore, cells stimulated with C_R3 showed low activation of STAT5 on differentiation day 5 (Fig. 6G). However, although the level of activation of STAT5 was still lower with C_R3 relative to EPO or A_R3, the level of STAT5 activation between A_dist_R5 and C_R3 was not significantly different ($P = 0.40$) on differentiation day 12, a time point when C_R3 began to perform better than A_dist_R5 (Fig. 6, B and G). This data suggests that biased signaling is affected by changes of EpoR dimer geometry in primary human erythroid cells. However, we have only surveyed a limited range of downstream effectors and thus may be missing specific signals that mediate the observed phenotypic effects. Our data suggests that this biased signaling is also dependent on the differentiation stage-specific context of the cells on which they act. The same agonists can result in different downstream signaling depending on cell state. The ability to modulate signaling through a single cytokine pathway at various stages of hematopoietic differentiation has broad applications in tuning desired responses for specific ligands.

Discussion

Although tunable signaling is a foundation of GPCR pharmacology that can be exploited through small-molecule medicinal chemistry, similar pharmacological principles have not been deeply explored for dimeric receptors that engage cytokines and growth factors because of the distinct structural challenges presented by the different systems. For GPCRs, signal modulation is achieved through small-molecule ligands that bind within pockets and induce different conformations of the GPCR helices within the membrane, resulting in differential activation of G proteins and arrestins (40). Structure-activity relationships for GPCR agonists can be obtained through medicinal chemistry. However, a comparable approach does not exist to explore signal tuning by the large class of Type-I transmembrane receptors, which require protein ligands to bind to large ECDs and induce large conformational changes that lead to dimerization. Although there have been hints that conformational changes that affect dimer topology may bias signaling (6, 15, 18, 24), the functional relevance has not been well characterized and is not well understood. We describe a general strategy to probe the effects of topological variation of receptor dimerization on signaling and function for cytokines and, in principle, any Type-I class receptor that signals as a dimer. This

new strategy allows tunable manipulation of geometric parameters, but there currently is no predictive framework to relate these geometric changes to signaling outcome. As such, the topological variation this system affords through protein ligand engineering can be analogized to exploration of small-molecule pharmacology by using medicinal chemistry.

Although the strategy itself is mechanistically agnostic, the signaling effects we observed in response to the topologically varied ligands are likely due to two factors. First, the orientational effects of the ECD could propagate to the ICDs that associate with the JAK2 kinases, affecting their relative proximities and orientations, which alters the efficiency by which JAK2 acts on its subsequent substrates on the EpoR ICD and STAT1, -3, and -5 (Figs. 4D and 5D and fig. S14). In different receptor topologies, the JAK2/ICD complexes are likely repositioned into orientations that are more or less conducive for transphosphorylation of the opposing JAK2 in the dimer, as well as tyrosine sites on the EpoR ICD. This could subsequently result in altered recruitment and/or phosphorylation of STATs and other adaptors that directly engage the JAK2 and ICD phospho-tyrosines, and these membrane-proximal phosphorylation differences will subsequently propagate to gene expression programs in the nucleus (41, 42). In general, the more extreme angles and distances result in less efficient downstream phosphorylation of all downstream adaptors to similar extents. However, uncoupling in the efficiency of JAK2 and STAT phosphorylation for some of the ligands—for example, A_R3, A_angle_R5, and A_dist_R5—results in the emergence of biased STAT activation.

A second explanation of the observed effects likely relates to mechanical distortion. As the topologies are forced into more extreme ranges, strain is induced in the system, resulting in fewer numbers of signaling complexes formed, with subsequent reduced receptor dimerization efficiency as observed with single-molecule assays, leading to lower E_{max} and right-shifted EC_{50} s and disproportionately affecting some second messengers more than others. Supporting this interpretation, there is a systematic pattern of reduced E_{max} that correlates with increasing dimer angle. For the distance series, there is no change in E_{max} until a sharp threshold, at which point it decreases abruptly. This could reflect a “rupture” distance at which point dimerized JAK2 molecules can no longer transphosphorylate efficiently. This rupture happens earlier with the angle series than with the distance series because the contortions needed to recover are greater. Possibly, both the angle and distance series interfere with weak, cooperative interactions between the transmembrane domains of EpoR that have been reported (34, 35).

As we have demonstrated for RBC biogenesis, this approach is suitable for examining how specific properties of cytokine signaling pathways may have differentiation-stage specificity in hematopoiesis or other aspects of cell dif-

ferentiation. This approach could also be used to survey cytokine receptor dimer geometries in order to identify signaling outputs of clinical interest in other cytokine receptor system, such as in the immune system. The scaffold we describe here could be used as a preclinical pharmacological tool to determine whether different degrees of agonism are optimal for a given cytokine in a particular therapeutic indication.

Materials and methods

EpoR protein expression and purification

The DNA encoding for EpoR ECD was cloned into pAcGP67-A, an insect cell protein expression vector. The vector includes a C-terminal 3C protease site, followed by a biotin-acceptor peptide tag (BAP tag, GLNDIFEAQKIEW), and a hexa-Histidine tag for affinity purification. The DNA encoding for the glycomutant of EpoR ECD-N46Q, N157Q (25) was also cloned into pAcGP67-A with a 6-His tag for affinity purification. The proteins were expressed using the baculovirus expression system. The baculovirus stocks were prepared by cotransfection of the BaculoSapphire DNA (Orbigen) and the pAcGP67-A DNA into *Spodoptera frugiperda* (Sf9). Next, the viruses were used to infect the *Trichoplusia ni* (High Five) cells. After 72 hours, the proteins were harvested from the supernatant and purified using nickel affinity chromatography (Nickel-NTA, Qiagen), followed by size-exclusion chromatography with a Superdex S200 column (GE Healthcare). The proteins were maintained in HEPES buffered saline (HBS, 20 mM HEPES pH 7.4, 150 mM sodium chloride). EpoR ECD was site-specifically biotinylated at the C-terminal BAP tag using *BirA* ligase and re-purified by size exclusion chromatography. Protein concentrations were determined by UV absorbance at 280 nm using a Nanodrop2000 spectrometer (Thermo Scientific), and then stored at -80°C .

DARPin expression and purification

The DNA encoding for the N2C and N3C DARPin proteins was cloned into pET-28 vector; a bacterial expression vector with a Kanamycin antibiotic resistance marker. The vector includes a C-terminal hexa-Histidine tag for affinity purification. The plasmids containing the gene of interest were used to transform Rosetta DE3 competent cells. The cells were grown at 37°C in 2YT media supplemented with Kanamycin (40 $\mu\text{g}/\text{mL}$) until the culture reached log-phase growth. Next, IPTG was added to the culture to induce protein expression at a final concentration of 1 mM. The culture was shaken at 37°C for 3 hours. Next, the proteins were harvested from the cells by sonication, and purified using nickel affinity chromatography, followed by size-exclusion chromatography with a Superdex S75 column (GE Healthcare). The proteins were maintained in phosphate-buffered saline (PBS, 135 mM NaCl, 2.5 mM KCl, 8.0 mM Na_2HPO_4 , 30 mM KH_2PO_4 , pH 7.2). Protein concentrations were determined by UV absorbance at 280 nm using a Nanodrop2000 spectrometer (Thermo Scientific), and then stored at -80°C .

The constructs for DARPin dimers based on the dimer C_R3 scaffold include an N-terminal hexa-Histidine tag for affinity purification. All of the extended DARPin proteins were maintained in Tris-buffered saline (50 mM Tris pH 8, 150 mM NaCl). The DARPin dimers A_dist_R5 through A_dist_R10, all of the mono-extended M_Rx DARPins, A_angle_R7, A_angle_R9, C_angle_R6, and C_angle_R8 were induced at 16°C for 16 to 18 hours.

Cell culture

The human UT7/EPO cells (32) were cultured in DMEM (Dulbecco's Modified Eagle Medium) supplemented with 10% v/v fetal bovine serum, penicillin-streptomycin, 1 mM L-glutamine, HEPES buffer, and 2 U/mL recombinant EPO (Amgen) (20). The cells were maintained at 37°C with 5% CO₂. The cultures were passaged every 2 to 3 days.

Yeast display of DARPins

DARPins were displayed on the surface of yeast *S. cerevisiae* strain EBY100 by fusion to the C terminus of the Aga2 protein. The DARPin insert, along with an N-terminal 3C protease cleavage site and a C-terminal cMyc epitope were cloned into the PCT302 vector. Briefly, competent yeast cells were electroporated with plasmids and recovered in SDCAA selection media at 30°C (43). Next, grown cultures were passaged in SDCAA media before inducing expression in SGCAA media. The cultures were induced at 30°C for 24 hours, followed by 20°C. The display of full-length DARPins on the surface of yeast was confirmed by staining the cells with an Alexa Fluor 488-labeled anti-cMyc antibody (1:100 dilution; Cell Signaling) and monitoring the fluorescence by flow cytometry.

Yeast displayed DARPin libraries

Two site-directed DARPin libraries (N2C and N3C) were created by assembly PCR using the following degenerate codons. The gel-purified assembled product was combined with linearized PCT302 vector and electroporated into EBY100 yeast cells (43). The electroporated yeast were recovered with SDCAA selection media and induced with SGCAA media, as described above.

N2C Library:

TCCGACCTGGGTAAGAACTGCTGGAAG-CAGCTCGTGCTGGTCAGGACGACGAAGTTCGT-ATCCTGATGGCTAATGGAGCAGATGTCAACGC-**GASW**GACN**WTDBGGT****TDY**ACTCCGCTG-CACCTGGCTGCT**MDSRHM**GGTACCTGGAAATCGTTGAAGTTTACTGAAGAACGGTGCTG-ACGTTAACGCT**ASW**GAT**NWTW****MC**GGA-**DY**GACACCACTTTCATCTAGCAGCG**AVW**-**MDS**GGACATCTCGAGATTGTCGAGGTCT-TACTCAAACACGGCGCAGACGTAATGCA-CAGGACAAATTCGGTAAGACCGCTTTCGATA-TCTCCATCGACAACGGTAACGAGGACCTGGC-TGAAATCCTGCAA

Theoretical diversity: 2.1×10^{10}

Diversity of library generated through electroporation: 1.8×10^9

N3C Library:

TCCGACCTGGGTAAGAACTGCTGGAAG-CAGCTCGTGCTGGTCAGGACGACGAAGTTCGT-ATCCTGATGGCTAATGGAGCAGATGTCAACGC-**GASW**GACN**WTDBGGT****TDY**ACTCCGCTG-CACCTGGCTGCT**MDSRHM**GGTACCTGGAAATCGTTGAAGTTTACTGAAGAACGGTGCTG-ACGTTAACGCT**ASW**GAT**NWTW****MC**GGA-**DY**GACACCACTTTCATCTAGCAGCG**AVW**-**MDS**GGACATCTCGAGATTGTCGAGGTCT-TACTCAAACACGGCGCAGACGTAATGCA-CAGGACAAATTCGGTAAGACCGCTTTCGATA-TCTCCATCGACAACGGTAACGAGGACCTGGC-TGAAATCCTGCAA

Theoretical diversity: 5.2×10^{11}

Diversity of library generated through electroporation: 1.0×10^9

Evolution of EpoR binding DARPins

The two yeast-displayed DARPin libraries (N2C and N3C) were panned against the EpoR ECD to select for high affinity clones using a combination of magnetic-activated cell sorting (MACS) and fluorescence-activated cell sorting (FACS). Biotinylated EpoR was used for all the selection rounds unless otherwise noted. The first round of selection was performed with 5.4×10^9 N2C and 5×10^9 N3C yeast cells to ensure coverage of library diversity. First, EpoR was mixed with 500 μ l of magnetic streptavidin microbeads (Miltenyi) to a final concentration of 400 nM. The mixture was then incubated with DARPin-displaying yeast cells at a final volume of 20 mL in PBE (PBS, 0.5% bovine serum albumin, 2 mM EDTA). The cells were incubated with shaking for 2 hours at 4°C. Next, the yeast cells were washed with PBE and flowed over MACS LS separation columns (Miltenyi) to isolate the EpoR binders. The enriched library pool was regrown in SDCAA media and then induced in SGCAA. In subsequent rounds, the total number of yeast cells used was ten times the number of yeast cells eluted in the previous round or 1×10^8 cells, whichever is larger.

For round 2, the on-bead selection with high avidity effects was repeated to select for more EpoR binders without increasing the stringency. EpoR was mixed with 250 μ l of magnetic streptavidin microbeads (Miltenyi) to a final concentration of 400 nM and incubated with yeast-displayed DARPin cells in 10 mL final volume. In round 3, the library pool (1×10^8 yeast cells) was incubated with Alexa Fluor 647-labeled anti-cMyc antibody, to enrich for transformants displaying full length DARPin clones. The mixture was incubated with shaking for 2 hours at 4°C, followed by PBE washes. The yeast cells were then incubated with anti-Alexa Fluor 647 microbeads (Miltenyi) and flowed over MACS LS separation columns to isolate the full-length clones.

In subsequent rounds, FACS method was employed to selectively enrich for EpoR binding clones. For round 4, the propagated and induced yeast cells from round 3 were incubated with

EpoR at a final concentration of 1 μ M monomer, in 1 mL PBE, with shaking for 2 hours at 4°C. The yeast cells were washed with PBE and then incubated with Alexa Fluor 488-labeled anti-cMyc antibody (Cell Signaling) and streptavidin-conjugated Alexa Fluor 647. The cells were then sorted using FACS to select for clones that exhibited high levels of EpoR binding (MFI of Alexa Fluor 647) relative to DARPin display levels (MFI of Alexa Fluor 488) on yeast.

Similarly, for the N2C library, the subsequent rounds of selections were performed at 333 nM, 40 nM and 4 nM EpoR concentrations for rounds 5, 6, and 7, respectively. Whereas, for the N3C library, the subsequent rounds of selections were performed at 333 nM, 10 nM and 4 nM EpoR concentrations for rounds 5, 6, and 7, respectively.

Second-generation library: Evolution of high-affinity DARPins

The two second generation DARPin libraries (N2C and N3C) containing DNA-shuffled clones were panned against biotinylated-EpoR ECD to select for high affinity clones, as described above. Diversities of the second-generation libraries generated through electroporation:

N2C library: 3.2×10^9

N3C library: 4.6×10^9

The first round of selections was performed with 1×10^{10} yeast, to ensure coverage of library diversity. For round 1, EpoR was mixed with 1000 μ l of magnetic streptavidin microbeads (Miltenyi) to a final concentration of 400 nM, and EpoR binding clones were isolated using MACS LS columns. For round 2, the library pools were incubated with 50 nM and 10 nM EpoR-tetramers for N2C and N3C libraries, respectively. The EpoR tetramers were generated by mixing biotinylated EpoR and streptavidin-conjugated Alexa Fluor 647, at a molar ratio of 4.5:1. Next, the yeast cells were incubated with EpoR-tetramers for 2 hours at 4°C. The yeast cells were then washed with PBE and incubated with anti-Alexa Fluor 647 microbeads. The EpoR binders were isolated using MACS LS separation columns.

To further enrich the library pool, FACS method was employed in subsequent rounds. For both the libraries, the subsequent rounds of selections were performed at 10 nM, 1 nM, and 0.1 nM EpoR concentrations for rounds 3, 4, and 5, respectively. For round 6, the library pool was subjected to a kinetic sort; a method to select for clones with slower off-rates. First, the library pools were incubated with 5 and 2.5 nM EpoR for N2C and N3C libraries, respectively. The yeast cells were washed and then dual-stained with Alexa Fluor 488-labeled anti-cMyc and streptavidin-conjugated Alexa Fluor 647. Next, a 100-fold excess of unbiotinylated EpoR, 500 nM for N2C and 250 nM for N3C in 1 mL was added to the cells. The mixture was shaken at room temperature, and the levels of bound protein were measured at regular intervals using flow cytometry. The levels did not change significantly over 21 hours. The cells were washed, retained, and then subjected to FACS.

Analysis of individual clones

To isolate individual clones, yeast cultures from the last selection rounds were plated on SDCAA agarose plates. Individual colonies were transferred to SDCAA media in culture tubes, passaged and then induced. Next, 93 clones were screened against a fixed EpoR concentration. For each clone, $\sim 5 \times 10^5$ cells were transferred to a V-bottom plate and incubated overnight with biotinylated EpoR at 4°C. The cells were washed and stained with streptavidin-conjugated Alexa Fluor 647. Next, the clones were analyzed for binding using flow cytometry. The highest affinity clones were identified, and their plasmids were isolated using the Zymoprep Yeast Plasmid Miniprep II Kit (Zymo Research), and sequenced. Yeast-displayed DARPin ligands were also titrated against EpoR at different concentrations to obtain EC_{50} values. As described above, $\sim 5 \times 10^5$ cells were transferred to a V-bottom plate and incubated with 100 μ L of serially diluted EpoR solution. Next, the cells were washed, stained, and then analyzed for EpoR binding by flow cytometry.

Surface plasmon resonance

Dissociation constants (K_d) for EpoR-binding DARPin ligands were determined by surface plasmon resonance (SPR) using the BIAcore T100 instrument (GE Healthcare). First, biotinylated EpoR was captured on a streptavidin-coated (SA) sensor chip (GE Healthcare) with immobilization density in the range of 100 resonance units (RU). Similarly, a control flow cell was also prepared with an off-target protein such as biotinylated-IFNAR1 or biotinylated-FzD8 for reference subtraction. The binding kinetics were performed at 25°C with a flow rate of 50 μ L/min. EpoR binding DARPin ligands were serially diluted in HBS buffer supplemented with 0.005% P20 surfactant (GE Healthcare) and injected over the SA chip. Dissociation kinetics were monitored for 200–500 s, as needed, based on the ligand affinity. For high affinity ligands, the chip was regenerated with 4 M $MgCl_2$ after each ligand injection. The binding kinetics and dissociation constants were determined using the BIAcore T100 evaluation software. The sensograms obtained were either fit to the 1:1 kinetic binding model or to the steady-state affinity model. The kinetic binding curves for each ligand were generated by plotting the time-dependent response units in Prism 7 (GraphPad).

Error-prone PCR

The EpoR binding individual clones obtained from the first set of selections were subjected to error prone PCR to introduce random mutations using the GeneMorph II Random Mutagenesis kit (Agilent). Various amounts of DNA template were tested to quantify the rate of mutagenesis. The GeneMorph kit was used at a concentration of 0.1 ng DNA/reaction, to achieve an average mutation rate of 2.5 to 3 mutations/gene. The PCR product was further amplified and purified by gel electrophoresis for DNA shuffling.

DNA shuffling

The EpoR binding clones with random mutations inserted through error-prone PCR were subjected to DNA shuffling (44) to enhance binding affinity. The amplified and purified DNA product from various clones was combined, and then used as the template for DNA shuffling. Briefly, 2 μ g of combined DNA was subjected to DNase treatment (DNase I, Invitrogen) by incubating at 15°C for three mins, followed by 80°C for 10 min to denature the enzyme. The DNA fragments were subjected to PCR clean-up (Qiagen) to remove extremely small fragments. Next, the fragments were allowed to recombine at regions of moderate homology. The PCR was performed using Taq (New England Biolabs) and PfuUltra (Agilent) polymerases with progressive hybridization. The reaction product was further amplified using PfuUltra polymerase. The product was purified using gel electrophoresis and the bands corresponding to N2C and N3C sizes were specifically extracted and purified. The gel-purified product was combined with linearized PCT302 vector and electroporated into EBY100 yeast cells to create the second-generation libraries. Diversity of library generated through electroporation:

N2C library: 3.2×10^9

N3C library: 4.6×10^9

Engineering the extended DARPins

The modular nature of the DARPin was utilized toward the generation of the extended DARPins. The DARPin molecules are non-planar, and each repeat provides a 2–3° counter-clockwise rotation relative to the preceding repeat (33). Thus, it is crucial to maintain the overall curvature of the DARPin to avoid a loss in binding affinity while inserting more ankyrin repeats. The sequence of the P repeat was carefully designed to maintain the curvature observed in the N3C E2 monomer, and the A_R3 and C_R3 dimers. The framework residues in the P repeat were based on the sequence of the consensus repeat. The positions that were randomized in the library design (denoted as X) (fig. S1) were assigned residues from a Frizzled8-binding DARPin. As a negative control, a DARPin dimer comprising of only non-binding P repeats was designed (NPPPPC) to eliminate the possibility of off-target (Frizzled8) effects. The control dimer shows no affinity toward EpoR or Frizzled8 (fig. S6).

As described above, the E2 DARPin is comprised of three EpoR binding repeats, denoted as “EEE,” and the N- and C-terminal capping regions. To engineer the “angle” series, one or more P repeats was inserted at the C terminus to provide DARPins such as NEEEP.C. Furthermore, the dimerizing repeats (indicated by underline) are placed on the same terminus as the P repeat insertions for maximum impact. In dimer A_R3/C_R3 (NEEEC), the dimerizing residues span over the three ankyrin repeats and the two capping regions. To generate A_angle_R4, one P repeat was inserted at the C-terminal end (NEEEPC) and the set of dimerizing residues were also shifted by one repeat. Similarly, the design for A_angle_R5 can be summarized as NEEEPC.

P repeat sequence: DAAGMTPLHLAAANGH-LEIVEVLLKYGADVNAK

To engineer the “distance” series, the non-binding P repeats were inserted at the N terminus, for example NPP...EEEC. Insertion of repeats at the N terminus proved challenging, as illustrated in fig. S9. A straightforward design based on the angle series such as NPEEEC displayed a significant loss in binding affinity toward EpoR. Three possible reasons were identified. First, an analysis of the models revealed a clash between residues of the inner helices from the first binding repeat and the preceding P repeat (fig. S7A). No such clashes were observed in the E2 DARPin where the N-terminal capping region helix precedes the first binding repeat (fig. S7B). Second, an analysis of the sequence of the E2 N-terminal capping region revealed a Glu to Lys mutation in the inner helix, which resulted from the error-prone mutagenesis performed during affinity maturation. The Lys residue is well positioned to interact with EpoR. Third, insertion of the P repeat implies existence of β -turn loops preceding the loop region from the first binding repeat. In E2, A_R3 (NEEEC) and the angle series, no β -turn loops precede the loop region for the first ankyrin repeat. The newly inserted loops could introduce destabilizing interactions. To address these issues, a modified repeat (P') was used as the repeat preceding the first E repeat such as NP..P'EEEC. In the P' repeat, the sequence of the inner helix was modified from HLAAANG to HKAARAG. The “KAARA” sequence is derived from the inner helix of the N-terminal capping region and installed in the P' repeat based on structural symmetry of the two helices. This eliminates the clashes between the helices and also re-positions the Lys residue to interact with EpoR. Furthermore, the loop region with the sequence DAAGM was shortened to Gly, to facilitate the turn while eliminating any destabilizing interactions, (fig. S7C). Increase in the loop length for DARPins has been previously published (45). Here, we show that the loops can also be shortened without affecting the structure for A_dist_R7 (fig. S7D). The dimerizing residues are now maintained at the N-terminal repeats. To generate A_dist_R4, P' repeat and the dimerizing residues were inserted at the N-terminal end (NP'EEEC). Whereas, to generate A_dist_R5, one P followed by one P' repeat was inserted, NPP'EEEC. Similarly, the design for A_dist_R6 can be summarized as NPPPP'EEEC. Also, the sequence of the P repeat used for generating the distance series is different from the P repeat used for the angle series (C-terminal insertions). But both the sequences are referred to as “P repeats” for the sake of simplicity.

P repeat sequence: DAAGTPLHHEAARAGH-LEIVEVLLKYGADVNAV

P' repeat sequence: DGTPLHKAARAGHLEIVEVLLKYGADVNAV

To engineer the “mono-extended” DARPin series, two sets of EpoR binding repeats were included on the same DARPin molecule. This series is based on monomeric extended DARPins, and thus named “mono-extended.” To generate

a series, the two sets of binding repeats were positioned at either termini, and the P repeats are inserted in the middle, for example NEEEEPP...EEEC. The second set of EpoR binding repeats are positioned similar to the distance series. Thus, the P' approach was adopted for the generation of the mono-extended series, as well. The insertion of one to four repeats in the middle showed severe clashes in the models generated. As a result, the first member of the series consisted of five non-binding repeats, M_R11, NEEEEPPPP'EEEC. Similarly, the design for M_R12 can be summarized as NEEEEPPPPPP'EEEC with a total of six non-binding repeats inserted.

P repeat sequence: DAAGGTPLHEAARAGHLEIVEVLLKYGADVNAV

P' repeat sequence: DGTPLHKAARAGHLEIVEVLLKYGADVNAV

Phospho-flow signaling assays

UT7/EPO cells were starved overnight for ~18 hours in base media without EPO. The cells were stimulated with EPO or the DARPIn ligands for 15 min at 37°C, followed by fixation with paraformaldehyde (Electron Microscopy Sciences) for 10 min at room temperature. Next, the cells were permeabilized for intracellular staining by treatment with methanol (Fisher) for 30 min at -20°C. The cells were then incubated with the desired antibodies at a 1:50 dilution for 1 hour at room temperature. The levels of the various phosphorylated proteins correspond to the measured values of mean fluorescence intensity (MFI). The background fluorescence of the unstimulated samples was subtracted from all the readouts. Data was acquired using CytoFlex, flow cytometer instrument (Beckman Coulter). The MFI values were normalized to the MFI of EPO at 37.04 nM and plotted in Prism 7 (GraphPad). The dose-response curves were generated using the "sigmoidal dose-response" analysis. A Gaussian distribution analysis was excluded as only some ligands demonstrate a decrease in MFI values at high concentrations. All the antibodies used were purchased from BD Biosciences: Alexa Fluor 488 Mouse Anti-Stat1 (pY701), Alexa Fluor 647 Mouse Anti-Stat3 (pY705), Alexa Fluor 488 Mouse Anti-Stat3 (pY705), Alexa Fluor 647 Mouse Anti-Stat5 (pY694), and Alexa Fluor 488 Mouse Anti-ERK1/2 (pT202/pY204).

Phosphorylated protein analysis

UT7/EPO cells were starved overnight and stimulated with saturating concentrations of EPO and DARPIn ligands for 15, 60, and 120 min at 37°C, followed by fixation with paraformaldehyde for 10 min at room temperature. Next, the cells were washed and resuspended in 0.5% bovine serum albumin in PBS, and stored at -80°C. The cells were then prepared for staining according to standard protocols. The cells were stained with a panel of antibodies (Primity Bio Pathway Phenotyping service) and analyzed on LSRII Flow cytometer (Becton Dickinson). The levels of phosphorylated protein were calculated as the Log (base 2) ratio of the MFI of stimulated samples to unstimulated samples.

Cell lysis and immunoprecipitation

UT7/EPO cells were starved overnight and stimulated with saturating concentrations of EPO (111 nM) and DARPIn ligands (1 μM) for 5 and 15 min at 37°C. Next, the cells were washed with ice-cold PBS and resuspended in 100 μl/5E6 cells lysis buffer and incubated with rotation for 30 min at 4°C. The Pierce IP lysis buffer (Thermo Scientific) was supplemented with phosphatase inhibitor cocktail (Abcam, 1/100 v/v), Halt phosphatase inhibitor cocktail (Thermo Scientific, 1/100 v/v), Sodium orthovanadate (NEB, 0.5 mM final concentration), and EDTA-free protease inhibitor cocktail (Roche, 1 tablet in 10 mL of buffer). The cell lysates were cleared by centrifugation at 10 krpm for 15 min at 4°C. The samples were denatured by the addition of 30 μl sample buffer (0.28 M Tris, pH 6.8; 30% v/v glycerol; 1% w/v SDS; 0.55 M β-mercaptoethanol; 0.0024% w/v bromophenol blue) and boiling for 5 min, resolved by 12.5% SDS-PAGE, and analyzed by immunoblotting.

For anti-EpoR immunoprecipitations, anti-EpoR antibody VP2E8 (Abcam, 4.6 μg/18E6 cells) was added to the clarified cell lysates and incubated with rotation for 1 hour at 4°C. Next, 30 μl of Pierce protein G magnetic beads (Thermo Scientific) were added, and incubated with rotation for 1 hour at 4°C. The beads were then washed three times with the supplemented lysis buffer. Next, the proteins were eluted by the addition of 160 μl sample buffer and boiling for 5 min. The beads were removed by magnetic separation. The samples were resolved by 12.5% SDS-PAGE and analyzed by immunoblotting. The antibodies used are as follows: Purified Mouse Anti-Stat1 (pY701, BD Biosciences), Rabbit anti-STAT1 42H3 (Cell Signaling Technology), Purified Mouse Anti-Stat5 (pY694, BD Biosciences), Rabbit anti-STAT5 3H7 (Cell Signaling Technology), anti-EpoR (VP2E8, Abcam), EpoR (D-5) HRP (sc365662, Santa Cruz Biotechnology), anti-JAK2 (EPR108[2], Abcam), anti-phospho(Y1007 + Y1008) JAK2 (E132, Abcam), phospho-EpoR Y426 (PA5-40305, Thermo Fisher Scientific), phospho-EpoR Y368 (PA5-38483, Thermo Fisher Scientific), phospho-EpoR Y456 (PA5-64795, Thermo Fisher Scientific), swine anti-rabbit immunoglobulins/HRP (P0399, Dako), and rabbit anti-mouse immunoglobulins/HRP (P0161, Dako).

Receptor internalization

UT7/EPO cells were starved overnight and then treated with 15 μg/mL cycloheximide (Sigma) for 4 hours. Next, the cells were stimulated with EPO (111 nM) or the DARPIn ligands (1 μM) for 15, 60, or 120 min at 37°C. The ligand solutions were also prepared in media containing cycloheximide. The cells were then washed with ice-cold PBS and incubated with anti-EpoR antibody for 1 hour at room temperature. Next, the cells were incubated with Alexa Fluor 647 goat anti-mouse antibody at a 1:100 dilution for 1 hour at room temperature. The levels of cell-surface EpoR correspond to the measured values of mean fluorescence intensity (MFI). The MFI values were normalized to the MFI of untreated

cells. The antibodies used are as follows: anti-EpoR (VP2E8, Abcam), Alexa Fluor 647 Goat anti-mouse (405322, Biolegend), and Alexa Fluor 647 Goat anti-mouse (A21235, Invitrogen).

Crystallization, data collection, and refinement

Protein complexes were formed by mixing 1:2 molar ratios of DARPIn and EpoR ECD (or 1:1 DARPIn/EpoR in the case of monomeric E2) along with Carboxypeptidases A and B at 1:100 (w/w), and phenylmethane sulfonyl fluoride at 0.5 mM final concentration. After overnight incubation at 4°C, complexes were purified by FPLC on an S200 column, eluted in HBS buffer, and concentrated. Crystallization was performed by sitting drop vapor diffusion using a Mosquito nanoliter pipetting robot. Monomeric E2-EpoR complex crystals were grown at 9 mg/mL from 1 M NaH₂PO₄/K₂HPO₄ pH 5.6. Crystals were cryoprotected by addition of ethylene glycol to 25% before harvesting for data collection at APS beamline 23 ID-B. C_R3 crystals were grown at 17 mg/mL from 0.1 M Tris pH 8.5, 25% PEG 3350, 1 mM reduced glutathione, and 1 mM oxidized glutathione. Crystals were cryoprotected by the addition of ethylene glycol to 25% before harvesting for data collection at SSRL beamline 12-2.

The C_R3/EpoR complex crystals were grown at 6 mg/mL from 0.1 M HEPES pH 7.3 and 1.4 M NaKHPO₄. Crystals were cryoprotected by the addition of glycerol to 24% before harvesting for data collection at ALS beamline 8.2.2. The A_angle_R5/EpoR complex was crystallized at 4.5 mg/mL from 0.2 M K/Na tartrate, 0.1 M Bis Tris propane pH 8.5, and 20% PEG 3350 and cryoprotected by the addition of glycerol to 30% before harvesting for data collection at ALS beamline 5.0.1. Crystals of the C_angle_R5/EpoR complex were grown at 6 mg/mL from 0.3 M MgSO₄, 0.1 M Bis-Tris Propane pH 7.0, and 22.5% PurePEGS cocktail (Anatrace) and cryoprotected by the addition of ethylene glycol to 30% before harvesting for data collection at ALS beamline 5.0.1. The A_dist_R7/EpoR complex was crystallized at 8 mg/mL from 0.2 M NaCl, 0.1 M Tris pH 8.5, and 25% PEG 3350 and harvested without further cryoprotection for data collection at ALS beamline 8.2.1. Initial crystals of the M_R12/EpoR complex were grown at 10 mg/mL from 0.2 M NaCl, 0.1 M CAPS pH 10.5, and 20% PEG 8000. These crystals were pulverized to form a seed stock for subsequent seeding into 0.2 M ammonium tartrate and 20% PEG 3350. The resulting crystals were dehydrated for 1 month by increasing the reservoir concentration to 25% PEG 3350. The crystals were cryoprotected by addition of 10% glycerol and 10% ethylene glycol before harvesting for data collection at APS beamline 23ID-B. All datasets were integrated and scaled using XDS (46) before merging symmetry-related reflections with aimless (47, 48). Due to anisotropy of the C_R3/EpoR, A_angle_R5/EpoR, C_angle_R5/EpoR, and M_R12/EpoR datasets, final ellipsoidal truncation was performed using STARaniso before merging reflections (49).

Structures were solved by molecular replacement with Phaser (50) using the crystal structure of EpoR [Protein Data Bank (PDB) ID 1ERN], split into D1 and D2 domains, and the predicted DARPin structures as search models, or in the case of the C_R3/EpoR complex using the refined C_R3 crystal structure. With the exceptions noted below, crystallographic models were prepared by iterative rounds of manual rebuilding and reciprocal space refinement with COOT (51) and Phenix (52–54). For the C_R3/EpoR, C_angle_R5/EpoR, and M_R12/EpoR complexes, additional refinement with Buster (55, 56) was performed to aid convergence of the structure before final refinement in Phenix. TLS refinement was performed for all structures except for the C_R3 dimer, for which anisotropic atomic displacement parameters (ADPs) were refined, and A_dist_R7/EpoR. Individual ADPs were refined for all structures except that grouped ADPs were refined for M_R12/EpoR and ADPs were not refined for A_dist_R7/EpoR. For the low-resolution A_dist_R7/EpoR structure, after molecular replacement the structure was manually edited in COOT to correct the amino acid sequence and to delete loop 4 of A_dist_R7, which was present in the search model but absent in the purified protein. Model refinement was then completed by rigid body refinement in Phenix and jelly body refinement in REFMAC (57–59). Software used in this project was installed and configured by SBGrid (60). Crystallographic data collection and refinement statistics along with PDB deposition codes are reported in tables S1 and S2.

Generation of models

The synthetic EpoR agonists described in this work have a unique property that differentiate them from previous efforts at generating synthetic type I cytokine agonists, namely they have fairly well-defined and rigid conformations that provide a structural basis for each observed physiological output. This advantage was leveraged by generating a crystallographic structure-informed set of signaling complex models for each of the A_dist_Rx, A_angle_Rx, and C_angle_Rx series. To best recapitulate both the backbone topology of the P repeat and the N-/C-terminal mode of EpoR binding, the backbone coordinates from the M_R12/EpoR crystal structure were used to construct each experimentally tested member of the extension series using the Rosetta macromolecular modeling suite. While most presented non-clashing complex models upon superposition of the E2-EpoR structure with the extended backbone, several cases showed significant clashes between EpoR subunits that could not be physically feasible. We used a constrained minimization protocol on each of the clashing complex models to generate a complete set of plausible models.

Backbone and symmetric complex generation

Backbone coordinates for each DARPin extension length were derived from the M_R12/EpoR structure while keeping capping modules intact. For A/C_angle, the N-terminal EpoR binding mode

was preserved from M_R12. For A_dist, the C-terminal EpoR binding mode was preserved which included the P' shortened loop modification which was impactful for binding. Each DARPin/EpoR complex was aligned to chain A of dimers A (pdb id 5HRY) and C (pdb id 5KBA). The synthetic signaling complex was generated in the Rosetta macromolecular modeling suite using a symmetry definition file to generate the C2 symmetry starting from each aligned DARPin/EpoR complex. The experimentally tested sequences were threaded to each backbone using the Rosetta packing algorithm with the default talaris2014 score function followed by side-chain energy minimization.

Relax of EpoR clashing models

Models that presented clashes between the membrane-proximal regions of the EpoR ECD were identified by visual inspection. An analysis of the EpoR conformation in all the crystal structures obtained singled residues 113–120 as a hinge region which allows for conformational flexibility between the binding domain and the membrane proximal domain. A Rosetta relax trajectory in search of a state with an energy minimum allowing backbone torsion angles to be modeled flexibly in this region while keeping the rest of the construct fixed using coordinate constraints was carried out for each clashing model. In the case of dimer A_R3, the first attempt with Rosetta relax to relieve the severe clashes between EpoR subunits was unsuccessful without having to make significant moves to the head region or rearranging the designed dimer interface orientation, so the EpoR conformation from A_angle_R5 was used instead for the relax trajectory. The relaxed output EpoR conformation from dimer A_R3 was used to rescue a non-clashing model for the A_angle_R4 complex. Although the generated non-clashing models do not represent unique solutions, they demonstrate the steric plausibility of a given complex.

Structural analysis of complex models

Although the synthetic agonists themselves are rather rigid, the EpoR ECD has some intrinsic flexibility between the D1 and D2 domains giving rise to uncertainty in measurements derived from models. Indeed, multiple EpoR conformers were observed in the crystal structures obtained for this work (fig. S10). Because the DARPin-EpoR D1 interaction is rigid, we made all distance and angle measurements using Val119 of EpoR, at the hinge between D1 and D2. Distance measurements between EpoR ECDs were made between the C α s of the residue Val119. Scissor half angle measurements were taken using Val119 of EpoR as the vertex with rays extending through Asp2 at the N-terminal cap of the DARPins and through an alanine at the start of the C-terminal cap of the DARPin (due to varying insertion lengths in DARPins with X repeats, this was residue number 39 + 33X). Although the measurements presented (Figs. 3 and 4) represent the general trend of complex geometries within the extension series, these measurements do not di-

rectly correspond to the relationship between the transmembrane or intracellular portions of EpoR in the cellular context.

Single molecule fluorescence imaging Sample preparation

HeLa cells were transiently transfected by calcium chloride precipitation with 10 μ g of pSems neo leader mXFP EpoR. In principle, a fluorescent-dead Green Fluorescent Protein (meGFP-Y66F/mXFP) was N-terminally fused to EpoR. After transfection, cells were seeded on a PLL-PEG-RGD coated glass cover slide (61). Imaging experiments were typically carried out 24h post transfection. Labeling, ligand incubation and subsequent imaging were performed in a custom-made incubation chamber with a volume of 500 μ l, which was mounted on the microscope. The experiments presented here were performed at room temperature in the presence of media without phenol red. Additionally, each sample was supplemented with an oxygen scavenger and a redox-active photo protectant to minimize photo bleaching (62). For cell surface labeling of mXFP-tagged EpoR DY647- and Rho11-labeled Nanobodies (NBs) were added in equal concentrations (2 nM each) and incubated for at least 5 min. High equilibrium binding of the labeled NBs was ensured by keeping these in bulk solution. Co-locomotion of EpoR was probed before and after incubating ligands at indicated concentrations for at least 10 min.

Single molecule microscopy

Single molecule imaging was performed by TIRF microscopy. As described previously (20, 24) an inverted microscope (Olympus IX71) equipped with a triple-line total internal reflection (TIR) condenser (Olympus) and a back-illuminated electron multiplied (EM) CCD camera (iXon DU897D, Andor Technology) was used. The sample was TIR illuminated via a 150x magnification objective with a numerical aperture of 1.45 (UAPO 150 x /1.45 TIRFM Olympus). Rho11 was excited by a 561 nm laser (CrystaLaser) at 0.95 mW (\sim 32 W/cm 2) and DY647 by a 642 nm laser (Omicron) at 0.65 mW (\sim 22W/cm 2). For fluorescent detection a spectral image splitter (Dual-View, Optical Insight) with a 640 DCXR dichroic beam splitter (Chroma) combined with a 580/40 (Semrock, Rho11 detection) and a 690/70 (Chroma, DY647 detection) bandpass filters has been used dividing each emission channel into 512 \times 256 pixel. For each cell image stacks of 150 frames were recorded with temporal resolution of approximately 32 ms/frame.

Single molecule analyses

The workflow of single molecule analyses is outlined in fig. S6A. Single molecule localization was assessed by using multiple-target tracing (MTT) algorithm (63) and tracking was performed, as described previously (64). Because immobile molecules (typically \sim 10% of the entire dataset) were mostly caused by either non-specific binding of labeled NBs to the coverslip or by endosomal uptake of receptors, these were identified by spatiotemporal cluster analysis (65) and

removed from the dataset. Dual-color co-tracking analysis was carried out as described recently (20). Prior to each experiment, RhoII and DY647 channels were aligned with sub-pixel precision based on a calibration with multicolor fluorescent beads (TetraSpeck microspheres 0.1 µm, Invitrogen). Individual molecules detected in both spectral channels within the same frame and within a distance threshold of 100 nm were considered as co-localized. In order to reconstruct co-locomotion trajectories (co-trajectories) from the identified population of co-localizing particles, the tracking algorithm was applied to the co-localization dataset. Co-trajectories with a minimum length of 10 consecutive steps (320 ms) were considered as receptor dimers. The relative fraction of co-locomotion was calculated with the absolute number of trajectories from both channels and was corrected for stochastically double labeling with the same fluorophore within a dimer. The relative fraction of co-locomoting particles was assessed with respect to the absolute number of tracked particles in both channels and corrected for stochastically double-labeled dimers by the same fluorophore species:

rel. co - locomotion =

$$\frac{2 * AB}{A + B} * \frac{1}{2 * \left[\left(\frac{A}{A+B} \right) * \left(\frac{B}{A+B} \right) \right]}$$

Where A, B, and AB are the absolute number of trajectories observed for RhoII and DY647 as well as co-trajectories, respectively (first part of the product determines the relative co-locomotion while the second part determines the correction factor for stochastically double labeling).

Human primary cell culture and analysis

CD34⁺ hematopoietic stem and progenitor cells from mobilized peripheral blood were purchased from the Fred Hutchinson Cancer Research Center. Primary cells were cultured as previously described (18). Cells were cultured with one of following ligands: EPO (3 U/mL), A_R3 (10 nM), A_angle_R4 (1 µM), A_angle_R5 (1 µM), A_angle_R6 (1 µM), C_R3 (10 nM), C_angle_R4 (100 nM), C_angle_R5 (100 nM), C_angle_R6 (100 nM), A_dist_R5 (333 nM), and A_dist_R7 (1 µM). Cell concentration was measured using an automated cell counter (Beckman Coulter). To evaluate erythroid differentiation, cells were stained with CD71-Fluorescein Isothiocyanate (FITC), CD11b/CD41a-Phycoerythrin (PE), and CD235a-Allophycocyanin (APC). Propidium Iodide (PI; 1:1,000) was used to discriminate live and dead cells. All antibodies were used at a 1:20 dilution, unless otherwise noted.

For phospho-STAT staining, differentiated primary erythroid cells were starved in cytokine-free media (1% BSA in IMDM) for 4 hours and stimulated either with EPO (3U/mL), A_R3 (10 nM), or A_dist_R5 (333 nM) for 1 hour. Treated cells were fixed and permeabilized as previously described (18). Then, cells were stained with Alexa Fluor-647 Mouse Anti-STAT5 (pY694; 1:20 dilution), Alexa Fluor-647 Mouse

Anti-STAT3 (pY705; 1:20 dilution), or Alexa Fluor-647 Mouse Anti-STAT1 (pY701; 1:20 dilution). Data were acquired using either BD Accuri C6 Cytometer or Canto instruments (Becton, Dickinson and Company) and all analysis was performed using FlowJo.

REFERENCES AND NOTES

- M. Akdis *et al.*, Interleukins (from IL-1 to IL-38), interferons, transforming growth factor β, and TNF-α: Receptors, functions, and roles in diseases. *J. Allergy Clin. Immunol.* **138**, 984–1010 (2016). doi: [10.1016/j.jaci.2016.06.033](https://doi.org/10.1016/j.jaci.2016.06.033); pmid: [27577879](https://pubmed.ncbi.nlm.nih.gov/27577879/)
- G. M. Delgoffe, P. J. Murray, D. A. Vignali, Interpreting mixed signals: The cell's cytokine conundrum. *Curr. Opin. Immunol.* **23**, 632–638 (2011). doi: [10.1016/j.coi.2011.07.013](https://doi.org/10.1016/j.coi.2011.07.013); pmid: [21852079](https://pubmed.ncbi.nlm.nih.gov/21852079/)
- J. B. Spangler, I. Moraga, J. L. Mendoza, K. C. Garcia, Insights into cytokine-receptor interactions from cytokine engineering. *Annu. Rev. Immunol.* **33**, 139–167 (2015). doi: [10.1146/annurev-immunol-032713-120211](https://doi.org/10.1146/annurev-immunol-032713-120211); pmid: [25493332](https://pubmed.ncbi.nlm.nih.gov/25493332/)
- K. Kaushansky, Lineage-specific hematopoietic growth factors. *N. Engl. J. Med.* **354**, 2034–2045 (2006). doi: [10.1056/NEJMr052706](https://doi.org/10.1056/NEJMr052706); pmid: [16687716](https://pubmed.ncbi.nlm.nih.gov/16687716/)
- R. M. Stroud, J. A. Wells, Mechanistic diversity of cytokine receptor signaling across cell membranes. *Sci. STKE* **2004**, re7 (2004). pmid: [15126678](https://pubmed.ncbi.nlm.nih.gov/15126678/)
- R. S. Syed *et al.*, Efficiency of signalling through cytokine receptors depends critically on receptor orientation. *Nature* **395**, 511–516 (1998). doi: [10.1038/26773](https://doi.org/10.1038/26773); pmid: [9774108](https://pubmed.ncbi.nlm.nih.gov/9774108/)
- M. Socolovsky, A. E. Fallon, H. F. Lodish, The prolactin receptor rescues EpoR^{-/-} erythroid progenitors and replaces EpoR in a synergistic interaction with c-kit. *Blood* **92**, 1491–1496 (1998). pmid: [9716574](https://pubmed.ncbi.nlm.nih.gov/9716574/)
- O. Livnah *et al.*, Functional mimicry of a protein hormone by a peptide agonist: The EPO receptor complex at 2.8 Å. *Science* **273**, 464–471 (1996). doi: [10.1126/science.273.5274.464](https://doi.org/10.1126/science.273.5274.464); pmid: [8662530](https://pubmed.ncbi.nlm.nih.gov/8662530/)
- M. A. Lemmon, J. Schlessinger, Cell signaling by receptor tyrosine kinases. *Cell* **141**, 1117–1134 (2010). doi: [10.1016/j.cell.2010.06.011](https://doi.org/10.1016/j.cell.2010.06.011); pmid: [20602996](https://pubmed.ncbi.nlm.nih.gov/20602996/)
- J. W. Adamson, Epoetin alfa: Into the new millennium. *Semin. Oncol.* **25**, 76–79 (1998). pmid: [9671336](https://pubmed.ncbi.nlm.nih.gov/9671336/)
- I. Moraga, J. Spangler, J. L. Mendoza, K. C. Garcia, Multifarious determinants of cytokine receptor signaling specificity. *Adv. Immunol.* **121**, 1–39 (2014). doi: [10.1016/B978-0-12-800100-4.00001-5](https://doi.org/10.1016/B978-0-12-800100-4.00001-5); pmid: [24388212](https://pubmed.ncbi.nlm.nih.gov/24388212/)
- K. Ozaki, W. J. Leonard, Cytokine and cytokine receptor pleiotropy and redundancy. *J. Biol. Chem.* **277**, 29355–29358 (2002). doi: [10.1074/jbc.R200003200](https://doi.org/10.1074/jbc.R200003200); pmid: [12072446](https://pubmed.ncbi.nlm.nih.gov/12072446/)
- J. T. Sockolovsky *et al.*, Selective targeting of engineered T cells using orthogonal IL-2 cytokine-receptor complexes. *Science* **359**, 1037–1042 (2018). doi: [10.1126/science.aar3246](https://doi.org/10.1126/science.aar3246); pmid: [29496879](https://pubmed.ncbi.nlm.nih.gov/29496879/)
- J. B. Mumm *et al.*, IL-10 elicits IFNγ-dependent tumor immune surveillance. *Cancer Cell* **20**, 781–796 (2011). doi: [10.1016/j.ccr.2011.11.003](https://doi.org/10.1016/j.ccr.2011.11.003); pmid: [22127223](https://pubmed.ncbi.nlm.nih.gov/22127223/)
- C. C. M. Ho *et al.*, Decoupling the functional pleiotropy of stem cell factor by tuning c-Kit signaling. *Cell* **168**, 1041–1052.e18 (2017). doi: [10.1016/j.cell.2017.02.011](https://doi.org/10.1016/j.cell.2017.02.011); pmid: [28283060](https://pubmed.ncbi.nlm.nih.gov/28283060/)
- C. Thomas *et al.*, Structural linkage between ligand discrimination and receptor activation by type I interferons. *Cell* **146**, 621–632 (2011). doi: [10.1016/j.cell.2011.06.048](https://doi.org/10.1016/j.cell.2011.06.048); pmid: [21854986](https://pubmed.ncbi.nlm.nih.gov/21854986/)
- S. Mitra *et al.*, Interleukin-2 activity can be fine tuned with engineered receptor signaling clamps. *Immunity* **42**, 826–838 (2015). doi: [10.1016/j.immuni.2015.04.018](https://doi.org/10.1016/j.immuni.2015.04.018); pmid: [25992859](https://pubmed.ncbi.nlm.nih.gov/25992859/)
- D. M. Freed *et al.*, EGFR ligands differentially stabilize receptor dimers to specify signaling kinetics. *Cell* **171**, 683–695.e18 (2017). doi: [10.1016/j.cell.2017.09.017](https://doi.org/10.1016/j.cell.2017.09.017); pmid: [28988771](https://pubmed.ncbi.nlm.nih.gov/28988771/)
- S. W. Rowlinson *et al.*, An agonist-induced conformational change in the growth hormone receptor determines the choice of signalling pathway. *Nat. Cell Biol.* **10**, 740–747 (2008). doi: [10.1038/ncb1737](https://doi.org/10.1038/ncb1737); pmid: [18488018](https://pubmed.ncbi.nlm.nih.gov/18488018/)
- A. R. Kim *et al.*, Functional selectivity in cytokine signaling revealed through a pathogenic EPO mutation. *Cell* **168**, 1053–1064.e15 (2017). doi: [10.1016/j.cell.2017.02.026](https://doi.org/10.1016/j.cell.2017.02.026); pmid: [28283061](https://pubmed.ncbi.nlm.nih.gov/28283061/)
- J. W. Wisler, K. Xiao, A. R. Thomsen, R. J. Lefkowitz, Recent developments in biased agonism. *Curr. Opin. Cell Biol.* **27**, 18–24 (2014). doi: [10.1016/j.cob.2013.10.008](https://doi.org/10.1016/j.cob.2013.10.008); pmid: [24680426](https://pubmed.ncbi.nlm.nih.gov/24680426/)

- M. D. Ballinger, J. A. Wells, Will any dimer do? *Nat. Struct. Biol.* **5**, 938–940 (1998). doi: [10.1038/2911](https://doi.org/10.1038/2911); pmid: [9808034](https://pubmed.ncbi.nlm.nih.gov/9808034/)
- J. Staerk *et al.*, Orientation-specific signalling by thrombopoietin receptor dimers. *EMBO J.* **30**, 4398–4413 (2011). doi: [10.1038/emboj.2011.315](https://doi.org/10.1038/emboj.2011.315); pmid: [21892137](https://pubmed.ncbi.nlm.nih.gov/21892137/)
- I. Moraga *et al.*, Tuning cytokine receptor signaling by re-orienting dimer geometry with surrogate ligands. *Cell* **160**, 1196–1208 (2015). doi: [10.1016/j.cell.2015.02.011](https://doi.org/10.1016/j.cell.2015.02.011); pmid: [25728669](https://pubmed.ncbi.nlm.nih.gov/25728669/)
- M. Kai *et al.*, Switching constant domains enhances agonist activities of antibodies to a thrombopoietin receptor. *Nat. Biotechnol.* **26**, 209–211 (2008). doi: [10.1038/nbt1376](https://doi.org/10.1038/nbt1376); pmid: [18157117](https://pubmed.ncbi.nlm.nih.gov/18157117/)
- H. Zhang *et al.*, Selecting agonists from single cells infected with combinatorial antibody libraries. *Chem. Biol.* **20**, 734–741 (2013). doi: [10.1016/j.chembiol.2013.04.012](https://doi.org/10.1016/j.chembiol.2013.04.012); pmid: [23706638](https://pubmed.ncbi.nlm.nih.gov/23706638/)
- K. Nakano *et al.*, Effective screening method of agonistic diabodies based on autocrine growth. *J. Immunol. Methods* **347**, 31–35 (2009). doi: [10.1016/j.jim.2009.05.012](https://doi.org/10.1016/j.jim.2009.05.012); pmid: [19508873](https://pubmed.ncbi.nlm.nih.gov/19508873/)
- A. Plückthun, Designed ankyrin repeat proteins (DARPs): Binding proteins for research, diagnostics, and therapy. *Annu. Rev. Pharmacol. Toxicol.* **55**, 489–511 (2015). doi: [10.1146/annurev-pharmtox-010611-134654](https://doi.org/10.1146/annurev-pharmtox-010611-134654); pmid: [25562645](https://pubmed.ncbi.nlm.nih.gov/25562645/)
- J. A. Fallas *et al.*, Computational design of self-assembling cyclic protein homo-oligomers. *Nat. Chem.* **9**, 353–360 (2017). doi: [10.1038/nchem.2673](https://doi.org/10.1038/nchem.2673); pmid: [28338692](https://pubmed.ncbi.nlm.nih.gov/28338692/)
- H. K. Binz, M. T. Stupp, P. Forrer, P. Amstutz, A. Plückthun, Designing repeat proteins: Well-expressed, soluble and stable proteins from combinatorial libraries of consensus ankyrin repeat proteins. *J. Mol. Biol.* **332**, 489–503 (2003). doi: [10.1016/S0022-2836\(03\)00896-9](https://doi.org/10.1016/S0022-2836(03)00896-9); pmid: [12948497](https://pubmed.ncbi.nlm.nih.gov/12948497/)
- H. K. Binz *et al.*, High-affinity binders selected from designed ankyrin repeat protein libraries. *Nat. Biotechnol.* **22**, 575–582 (2004). doi: [10.1038/nbt962](https://doi.org/10.1038/nbt962); pmid: [15097997](https://pubmed.ncbi.nlm.nih.gov/15097997/)
- N. Komatsu *et al.*, Establishment and characterization of a human leukemic cell line with megakaryocytic features: Dependency on granulocyte-macrophage colony-stimulating factor, interleukin 3, or erythropoietin for growth and survival. *Cancer Res.* **51**, 341–348 (1991). pmid: [1824823](https://pubmed.ncbi.nlm.nih.gov/1824823/)
- J. Li, A. Mahajan, M.-D. Tsai, Ankyrin repeat: A unique motif mediating protein-protein interactions. *Biochemistry* **45**, 15168–15178 (2006). doi: [10.1021/bi062188g](https://doi.org/10.1021/bi062188g); pmid: [17176038](https://pubmed.ncbi.nlm.nih.gov/17176038/)
- A. Z. Ebie, K. G. Fleming, Dimerization of the erythropoietin receptor transmembrane domain in micelles. *J. Mol. Biol.* **366**, 517–524 (2007). doi: [10.1016/j.jmb.2006.11.035](https://doi.org/10.1016/j.jmb.2006.11.035); pmid: [17173930](https://pubmed.ncbi.nlm.nih.gov/17173930/)
- S. N. Constantinescu *et al.*, The erythropoietin receptor transmembrane domain mediates complex formation with viral anemic and polythetic gp55 proteins. *J. Biol. Chem.* **278**, 43755–43763 (2003). doi: [10.1074/jbc.M302974200](https://doi.org/10.1074/jbc.M302974200); pmid: [12930840](https://pubmed.ncbi.nlm.nih.gov/12930840/)
- F. C. Giani *et al.*, Targeted application of human genetic variation can improve red blood cell production from stem cells. *Cell Stem Cell* **18**, 73–78 (2016). doi: [10.1016/j.stem.2015.09.015](https://doi.org/10.1016/j.stem.2015.09.015); pmid: [26607381](https://pubmed.ncbi.nlm.nih.gov/26607381/)
- J. Hu *et al.*, Isolation and functional characterization of human erythroblasts at distinct stages: Implications for understanding of normal and disordered erythropoiesis in vivo. *Blood* **121**, 3246–3253 (2013). doi: [10.1182/blood-2013-01-476390](https://doi.org/10.1182/blood-2013-01-476390); pmid: [23422750](https://pubmed.ncbi.nlm.nih.gov/23422750/)
- D. Metcalf, Hematopoietic cytokines. *Blood* **111**, 485–491 (2008). doi: [10.1182/blood-2007-03-079681](https://doi.org/10.1182/blood-2007-03-079681); pmid: [18182579](https://pubmed.ncbi.nlm.nih.gov/18182579/)
- U. Testa, Apoptotic mechanisms in the control of erythropoiesis. *Leukemia* **18**, 1176–1199 (2004). doi: [10.1038/sj.leu.2403383](https://doi.org/10.1038/sj.leu.2403383); pmid: [15208642](https://pubmed.ncbi.nlm.nih.gov/15208642/)
- D. Winkpeny, M. Clark, D. Cawkliff, Biased ligand quantification in drug discovery: From theory to high throughput screening to identify new biased μ opioid receptor agonists. *Br. J. Pharmacol.* **173**, 1393–1403 (2016). doi: [10.1111/bph.13441](https://doi.org/10.1111/bph.13441); pmid: [26791140](https://pubmed.ncbi.nlm.nih.gov/26791140/)
- M. J. Waters, A. J. Brooks, JAK2 activation by growth hormone and other cytokines. *Biochem. J.* **466**, 1–11 (2015). doi: [10.1042/BJ20141293](https://doi.org/10.1042/BJ20141293); pmid: [25656053](https://pubmed.ncbi.nlm.nih.gov/25656053/)
- R. D. Ferrao, H. J. Wallweber, P. J. Lupardus, Receptor-mediated dimerization of JAK2 FERM domains is required for JAK2 activation. *eLife* **7**, e38089 (2018). doi: [10.7554/eLife.38089](https://doi.org/10.7554/eLife.38089); pmid: [30044226](https://pubmed.ncbi.nlm.nih.gov/30044226/)
- G. Chao *et al.*, Isolating and engineering human antibodies using yeast surface display. *Nat. Protoc.* **1**, 755–768 (2006). doi: [10.1038/nprot.2006.94](https://doi.org/10.1038/nprot.2006.94); pmid: [17406305](https://pubmed.ncbi.nlm.nih.gov/17406305/)

44. A. J. Meyer, J. W. Ellefson, A. D. Ellington, *Curr. Protoc. Mol. Biol.* **105**, 15.21.1–15.12.7 (2014).
45. J. Schilling, J. Schöppe, A. Plückthun, From DARPins to LoopDARPins: Novel LoopDARPin design allows the selection of low picomolar binders in a single round of ribosome display. *J. Mol. Biol.* **426**, 691–721 (2014). doi: [10.1016/j.jmb.2013.10.026](https://doi.org/10.1016/j.jmb.2013.10.026); pmid: [24513107](https://pubmed.ncbi.nlm.nih.gov/24513107/)
46. W. Kabsch, XDS. *Acta Crystallogr. D Biol. Crystallogr.* **66**, 125–132 (2010). doi: [10.1107/S0907444909047337](https://doi.org/10.1107/S0907444909047337); pmid: [20124692](https://pubmed.ncbi.nlm.nih.gov/20124692/)
47. P. R. Evans, An introduction to data reduction: Space-group determination, scaling and intensity statistics. *Acta Crystallogr. D Biol. Crystallogr.* **67**, 282–292 (2011). doi: [10.1107/S090744491003982X](https://doi.org/10.1107/S090744491003982X); pmid: [21460446](https://pubmed.ncbi.nlm.nih.gov/21460446/)
48. M. D. Winn et al., Overview of the CCP4 suite and current developments. *Acta Crystallogr. D Biol. Crystallogr.* **67**, 235–242 (2011). doi: [10.1107/S0907444910045749](https://doi.org/10.1107/S0907444910045749); pmid: [21460441](https://pubmed.ncbi.nlm.nih.gov/21460441/)
49. J. F. Bruhn et al., Crystal structure of the Marburg virus VP35 oligomerization domain. *J. Virol.* **91**, e01085-16 (2017). doi: [10.1128/JVI.01085-16](https://doi.org/10.1128/JVI.01085-16); pmid: [27847355](https://pubmed.ncbi.nlm.nih.gov/27847355/)
50. A. J. McCoy et al., Phaser crystallographic software. *J. Appl. Crystallogr.* **40**, 658–674 (2007). doi: [10.1107/S0021889807021206](https://doi.org/10.1107/S0021889807021206); pmid: [19461840](https://pubmed.ncbi.nlm.nih.gov/19461840/)
51. P. Emsley, B. Lohkamp, W. G. Scott, K. Cowtan, Features and development of Coot. *Acta Crystallogr. D Biol. Crystallogr.* **66**, 486–501 (2010). doi: [10.1107/S0907444910007493](https://doi.org/10.1107/S0907444910007493); pmid: [20383002](https://pubmed.ncbi.nlm.nih.gov/20383002/)
52. P. D. Adams et al., PHENIX: A comprehensive Python-based system for macromolecular structure solution. *Acta Crystallogr. D Biol. Crystallogr.* **66**, 213–221 (2010). doi: [10.1107/S0907444909052925](https://doi.org/10.1107/S0907444909052925); pmid: [20124702](https://pubmed.ncbi.nlm.nih.gov/20124702/)
53. T. C. Terwilliger et al., Iterative model building, structure refinement and density modification with the PHENIX AutoBuild wizard. *Acta Crystallogr. D Biol. Crystallogr.* **64**, 61–69 (2008). doi: [10.1107/S090744490705024X](https://doi.org/10.1107/S090744490705024X); pmid: [18094468](https://pubmed.ncbi.nlm.nih.gov/18094468/)
54. P. V. Afonine et al., Towards automated crystallographic structure refinement with phenix.refine. *Acta Crystallogr. D Biol. Crystallogr.* **68**, 352–367 (2012). doi: [10.1107/S0907444912001308](https://doi.org/10.1107/S0907444912001308); pmid: [22505256](https://pubmed.ncbi.nlm.nih.gov/22505256/)
55. G. Bricogne et al., BUSTER version 2.10.3. *Cambridge, United Kingdom Glob. Phasing Ltd* (2016).
56. O. S. Smart et al., Exploiting structure similarity in refinement: Automated NCS and target-structure restraints in BUSTER. *Acta Crystallogr. D Biol. Crystallogr.* **68**, 368–380 (2012). doi: [10.1107/S0907444911056058](https://doi.org/10.1107/S0907444911056058); pmid: [22505257](https://pubmed.ncbi.nlm.nih.gov/22505257/)
57. R. A. Nicholls, F. Long, G. N. Murshudov, Low-resolution refinement tools in REFMAC5. *Acta Crystallogr. D Biol. Crystallogr.* **68**, 404–417 (2012). doi: [10.1107/S090744491105606X](https://doi.org/10.1107/S090744491105606X); pmid: [22505260](https://pubmed.ncbi.nlm.nih.gov/22505260/)
58. G. N. Murshudov et al., REFMAC5 for the refinement of macromolecular crystal structures. *Acta Crystallogr. D Biol. Crystallogr.* **67**, 355–367 (2011). doi: [10.1107/S0907444911001314](https://doi.org/10.1107/S0907444911001314); pmid: [21460454](https://pubmed.ncbi.nlm.nih.gov/21460454/)
59. O. Kovalevskiy, R. A. Nicholls, G. N. Murshudov, Automated refinement of macromolecular structures at low resolution using prior information. *Acta Crystallogr. D Struct. Biol.* **72**, 1149–1161 (2016). doi: [10.1107/S2059798316014534](https://doi.org/10.1107/S2059798316014534); pmid: [27710936](https://pubmed.ncbi.nlm.nih.gov/27710936/)
60. A. Morin et al., Cutting edge: Collaboration gets the most out of software. *eLife* **2**, e01456 (2013). doi: [10.7554/eLife.01456](https://doi.org/10.7554/eLife.01456); pmid: [24040512](https://pubmed.ncbi.nlm.nih.gov/24040512/)
61. S. Wilmes et al., Receptor dimerization dynamics as a regulatory valve for plasticity of type I interferon signaling. *J. Cell Biol.* **209**, 579–593 (2015). doi: [10.1083/jcb.201412049](https://doi.org/10.1083/jcb.201412049); pmid: [26008745](https://pubmed.ncbi.nlm.nih.gov/26008745/)
62. J. Vogelsang et al., A reducing and oxidizing system minimizes photobleaching and blinking of fluorescent dyes. *Angew. Chem. Int. Ed.* **47**, 5465–5469 (2008). doi: [10.1002/anie.200801518](https://doi.org/10.1002/anie.200801518); pmid: [18601270](https://pubmed.ncbi.nlm.nih.gov/18601270/)
63. A. Sergé, N. Bertaux, H. Rigneault, D. Marguet, Dynamic multiple-target tracing to probe spatiotemporal cartography of cell membranes. *Nat. Methods* **5**, 687–694 (2008). doi: [10.1038/nmeth.1233](https://doi.org/10.1038/nmeth.1233); pmid: [18604216](https://pubmed.ncbi.nlm.nih.gov/18604216/)
64. K. Jaqaman et al., Robust single-particle tracking in live-cell time-lapse sequences. *Nat. Methods* **5**, 695–702 (2008). doi: [10.1038/nmeth.1237](https://doi.org/10.1038/nmeth.1237); pmid: [18641657](https://pubmed.ncbi.nlm.nih.gov/18641657/)
65. F. Roder, S. Wilmes, C. P. Richter, J. Piehler, Rapid transfer of transmembrane proteins for single molecule dimerization assays in polymer-supported membranes. *ACS Chem. Biol.* **9**, 2479–2484 (2014). doi: [10.1021/cb5005806](https://doi.org/10.1021/cb5005806); pmid: [25203456](https://pubmed.ncbi.nlm.nih.gov/25203456/)

ACKNOWLEDGMENTS

We thank A. Velasco for assistance. We thank I. Tickle for assistance with x-ray data processing. **Funding:** This work was supported by NIH R01-AI51321 (K.C.G.), NIH T32HL066987 (A.R.K.), NIH R01 DK103794, and R33 HL120791 (V.G.S.); Deutsche Forschungsgemeinschaft (DFG) SFB 944 (J.P.); a gift from the Mathers Fund (K.C.G.); and the Howard Hughes Medical Institute (HHMI) (D.B. and K.C.G.). GM/CA@APS has been funded in whole or in part with federal funds from the National Cancer Institute (ACB-12002) and the National Institute of General Medical Sciences (NIGMS) (AGM-12006). This research used resources of the Advanced Photon Source, a U.S. Department of Energy (DOE) Office of Science User Facility operated for the DOE Office of Science by Argonne National Laboratory under contract DE-AC02-06CH11357. The Eiger 16M detector was funded by an NIH–Office of Research Infrastructure Programs, High-End Instrumentation Grant (1S100D012289-01A1). The Berkeley Center for Structural Biology is supported in part by HHMI. The Advanced Light

Source is a DOE Office of Science User Facility under contract DE-AC02-05CH11231. The Pilatus detector on 5.0.1 was funded under NIH grant S100D021832. Use of the Stanford Synchrotron Radiation Lightsource (SSRL), SLAC National Accelerator Laboratory, is supported by the DOE Office of Science, Office of Basic Energy Sciences under contract DE-AC02-76SF00515. The SSRL Structural Molecular Biology Program is supported by the DOE Office of Biological and Environmental Research and by the NIH and NIGMS (including P41GM103393). **Author contributions:** K.C.G. conceived of the project. K.M., G.U., J.A.F., D.B., and K.C.G. jointly developed the approach for tuning receptor engagement geometry with extendable scaffolds through an iteration of computational design (G.U., J.A.F., and D.B.) and protein engineering (K.M. and K.C.G.). K.M. designed and constructed the DARPin libraries, performed yeast-display selections and affinity maturation, designed and generated the sequences for the extended DARPins, expressed recombinant proteins, biophysically and functionally characterized all the DARPins, and performed immunoprecipitation and protein immunoblotting experiments. G.U. and J.A.F. designed the initial two dimer interfaces. G.U. worked with K.M. to design sequences for the extended DARPin/EpoR complexes and generated three-dimensional models of these complexes. A.R.K. performed the erythropoiesis experiments. K.M., K.M.J., and Y.G. crystallized the protein complexes. K.M.J. and Y.G. collected the crystallography data and determined structures. M.H. performed the TIRF microscopy experiments. Y.M. provided the reference proteins for SPR. R.A.S. assisted with immunoblot analysis. J.P. supervised the TIRF microscopy experiments. V.G.S. supervised the erythropoiesis experiments. K.C.G. and D.B. supervised the project and interpreted the data. K.M. and K.C.G. wrote the manuscript with inputs from all authors. **Competing interests:** K.C.G., D.B., K.M., G.U., K.M.J., and J.A.F. are inventors on U.S. patent application 62/819,645 titled “topological control of receptor signaling using synthetic homo- and hetero-dimeric cytokine mimetics.” **Data and materials availability:** Coordinates and structure factors of the complex have been deposited in the Protein Data Bank with accession codes 6MOE, 6MOG, 6MOH, 6MOI, 6MOJ, 6MOK, and 6MOL. Diffraction images have been deposited in the SGrid Data Bank. All other data are available in the manuscript or the supplementary materials.

SUPPLEMENTARY MATERIALS

science.sciencemag.org/content/364/6442/eaav7532/suppl/DC1
Figs. S1 to S18
Tables S1 to S5
Reference (66)
Movies S1 and S2

16 October 2018; accepted 8 April 2019
10.1126/science.aav7532

Topological control of cytokine receptor signaling induces differential effects in hematopoiesis

Kritika Mohan, George Ueda, Ah Ram Kim, Kevin M. Jude, Jorge A. Fallas, Yu Guo, Maximillian Hafer, Yi Miao, Robert A. Saxton, Jacob Piehler, Vijay G. Sankaran, David Baker and K. Christopher Garcia

Science **364** (6442), eaav7532.
DOI: 10.1126/science.aav7532

Exploring a range of signaling

Cytokines are small proteins that bind to the extracellular domains of transmembrane receptors to activate signaling pathways inside the cell. They often act by dimerizing their receptors, and changes in dimer orientation of the extracellular domains can change the signaling output. Mohan *et al.* systematically explored this tuning effect by designing a series of dimer ligands for the erythropoietin receptor in which they varied the distance and angle between monomers. The topology affected the strength of activation and differentially affected different pathways, which raises the potential for exploiting such ligands in medicinal chemistry.

Science, this issue p. eaav7532

ARTICLE TOOLS

<http://science.sciencemag.org/content/364/6442/eaav7532>

SUPPLEMENTARY MATERIALS

<http://science.sciencemag.org/content/suppl/2019/05/22/364.6442.eaav7532.DC1>

REFERENCES

This article cites 65 articles, 13 of which you can access for free
<http://science.sciencemag.org/content/364/6442/eaav7532#BIBL>

PERMISSIONS

<http://www.sciencemag.org/help/reprints-and-permissions>

Use of this article is subject to the [Terms of Service](#)